Phosphoproteomic analysis identifies supervillin as an ERK3 substrate regulating cytokinesis and cell ploidy

Joaquim Javary[1*], Eugénie Goupil[1*], Mathilde Soulez[1], Evgeny Kanshin[1,2,7], Antoine Bouchard[1,8], Ole-Morten Seternes[3], Pierre Thibault[1,2], Jean-Claude Labbé[1,4,5] and Sylvain Meloche[1,4,6]

[1]Institute for Research in Immunology and Cancer, Montreal, Quebec H3T 1J4, Canada
[2]Department of Chemistry, Faculty of Arts and Sciences, Université de Montréal, Montreal, Quebec H3T 1J4, Canada
[3]Department of Pharmacy, UiT The Arctic University of Norway, N-9037 Tromso, Norway
[4]Molecular Biology Program, Faculty of Medicine, Université de Montréal, Montreal, Quebec H3T 1J4, Canada
[5]Department of Pathology and Cell Biology, Faculty of Medicine, Université de Montréal, Montreal, Quebec H3T 1J4, Canada
[6]Department of Pharmacology and Physiology, Faculty of Medicine, Université de Montréal, Montreal, Quebec H3T 1J4, Canada

[7]Present address: NYU Langone Health, New York, USA
8Present address: Institut de recherches cliniques de Montréal, Montreal, Quebec, Canada

[*]These authors contributed equally to this work

Running title: ERK3 phosphorylates SVIL in mitosis

Correspondence: Dr Sylvain Meloche
Institute for Research in Immunology and Cancer
2950, Chemin de Polytechnique
Montreal, QC H3C 3J7, Canada
Email: sylvain.meloche@umontreal.ca

ABSTRACT

Extracellular signal-regulated kinase 3 (ERK3) is a poorly characterized member of the mitogen-activated protein (MAP) kinase family. Functional analysis of the ERK3 signaling pathway has been hampered by a lack of knowledge about the substrates and downstream effectors of the kinase. Here, we used large-scale quantitative phosphoproteomics and targeted gene silencing to identify direct ERK3 substrates and gain insight into its cellular functions. Detailed validation of one candidate substrate identified the gelsolin/villin family member supervillin (SVIL) as a *bona fide* ERK3 substrate. We show that ERK3 phosphorylates SVIL on Ser245 to regulate myosin II activation and cytokinesis completion in dividing cells. Depletion of SVIL or ERK3 leads to increased cytokinesis failure and multinucleation, a phenotype rescued by wild type SVIL but not by the non-phosphorylatable S245A mutant. Our results unveil a new function of the atypical MAP kinase ERK3 in cell division and the regulation of cell ploidy.

Keywords: cell division, ERK3, MAP kinases, phosphoproteomics, signal transduction, supervillin

INTRODUCTION

Extracellular signal-regulated kinase 3 (ERK3) along with its paralog ERK4 define a distinct subfamily of atypical mitogen-activated protein (MAP) kinases (Coulombe and Meloche, 2007; Cargnello and Roux, 2011). By contrast to the classical MAP kinases ERK1/2, JNK1/2/3, p38α/β/γ/δ and ERK5, which are activated by dual phosphorylation of the Thr-Xxx-Tyr motif in the activation loop of the kinase domain, ERK3 and ERK4 contain a single phospho-acceptor site in their activation loop and are not substrates of MAP kinase kinases. Much remains to be learned about the regulation, substrate repertoire and functions of these protein kinases. ERK3 is phosphorylated on activation loop Ser189 by group I p21-activated kinases and displays constitutive enzymatic activity in most cell types (Déleris et al., 2008; De La Mota-Peynado et al., 2011; Déléris et al., 2011). It has been postulated that ERK3 activity is regulated, at least in part, by its cellular abundance through the control of protein turnover (Coulombe et al., 2003). Notably, ERK3 is phosphorylated by cyclin B-CDK1 during mitosis entry leading to its stabilization and transient accumulation (Tanguay et al., 2010), although the functional consequence of this regulation is unknown.

Unlike classical MAP kinases, which are multifunctional Ser/Thr kinases that phosphorylate hundreds of protein substrates (Ünal et al., 2017; Trempolec et al., 2013; Zeke et al., 2016), ERK3 does not phosphorylate generic MAP kinase substrates, suggesting a more restricted substrate specificity (Cheng et al., 1996). To date, the only physiologically validated substrate of ERK3 is the MAP kinase-activated protein kinase (MK) family member MK5 (Seternes et al., 2004; Schumacher et al., 2004; Déleris et al., 2008). Of note, classical MAP kinases bind to downstream MKs and other substrates via a cluster of negatively charged amino acids, known as the common docking (CD) domain, found in the C-terminal half of the kinase domain (Tanoue et al., 2000). However, the CD domain of ERK3 is dispensable for its interaction with MK5. Instead, ERK3 binding to MK5 is mediated by a FRIEDE motif localized

in the C34 domain (Coulombe and Meloche, 2007), which is essential for MK5 activating phosphorylation (Åberg et al., 2009). This mechanism may contribute to the difference in substrate selection between ERK3 and classical MAP kinases.

Studies with genetically-engineered mice have revealed that mice lacking ERK3 kinase activity or expression are born at normal mendelian frequency and survive to adulthood without any apparent health issue (Soulez et al., 2019). However, ERK3 kinase activity is required for optimal post-natal myogenesis and muscle regeneration by stimulating the proliferation of skeletal muscle myogenic progenitors (Soulez et al., 2022). Mice deficient in ERK4 are also viable and fertile and exhibit no gross physiological anomaly (Rousseau et al., 2010). Cellular studies point to important roles for ERK3 signaling in the regulation of cytoskeletal dynamics, cell migration and invasion, cell proliferation, and transcriptional control. Overexpression of ERK3 in epithelial cells induces a reorganization of the actin cytoskeleton, associated with a decrease in the number of stress fibers and reduced cellular adhesion (Al-Mahdi et al., 2015; Mathien et al., 2017). Consistently, ERK3 signaling enhances cellular migration in different epithelial and endothelial cell types (Long et al., 2012; Al-Mahdi et al., 2015; Mathien et al., 2017; Wang et al., 2014; Elkhadragy et al., 2017). ERK3 was also shown to stimulate leukocytes chemotaxis by inducing the transcription of *CXCL8* and other chemokine-encoding genes (Bogucka et al., 2020). However, the downstream effectors and molecular mechanisms underlying these functions of ERK3 remain largely unknown. Interestingly, evidence is accumulating that ERK3 signaling may contribute to tumor progression. Indeed, ERK3 was reported to promote cancer cell invasion and metastasis, clonogenic cell proliferation, and tumor growth in xenograft models (Long et al., 2012; Bogucka et al., 2020; Cai et al., 2021). These observations further highlight the importance of defining the substrate repertoire of ERK3 to elucidate its cellular functions.

To identify novel substrates of ERK3, we performed a large-scale quantitative phosphoproteomic analysis of breast cancer epithelial cells after genetic depletion of ERK3. This led to the identification of supervillin (SVIL) as a candidate substrate of ERK3. SVIL is the largest member of the gelsolin/villin family of actin-binding proteins (Nag et al., 2013). It is a multi-domain protein that interacts with F-actin, myosin II and other cytoskeletal proteins to regulate cellular adhesion, cell motility, podosome turnover, and matrix invasion (Takizawa et al., 2006, 2007; Fang et al., 2010; Crowley et al., 2009; Bhuwania et al., 2012). SVIL is also required for cytokinesis (Smith et al., 2010, 2013). We validated that ERK3 phosphorylates SVIL on Ser245 *in vitro* and in intact cells, a modification that is required for normal execution of cytokinesis. Our results uncover SVIL as a novel substrate of ERK3 and further implicate this atypical MAP kinase in the regulation of cytokinesis and cell ploidy.

MATERIALS AND METHODS

Reagents, plasmids and antibodies

Recombinant active ERK1 was purchased from Millipore (cat# 14-439). Recombinant active CDK1/cyclin B1 (cat# C22-10G) and histone H1 (cat# H10-54N) were obtained from SignalChem. Lambda protein phosphatase was obtained from New England Biolabs (cat# P0753S). Myelin basic protein (MBP) (cat# M1891), thymidine (cat# T9250), RO-3306 (cat# SML0569), nocodazole (cat# 487928), and MG-132 (cat# M8699) were purchased from Sigma-Aldrich. The small molecule ERK3 inhibitor [3-(4-Methoxy-phenyl)-3H-[1,2,3]triazolo[4,5-d]pyrimidin-5-yl]-((R)-1-pyridin-4-yl-pyrrolidin-3-yl)-amine (compound 18) was synthesized in-house as described (Grädler et al., 2020).

Plasmids pcDNA3-Myc_6-ERK3 and pcDNA3-Myc_6-ERK3 K49/K50 (KD) have been previously described (Coulombe et al., 2003). Plasmids encoding ERK3 deletion constructs pcDNA3-Myc_6-ERK3(1-365) (N-terminus) and pcDNA3-Myc_6-ERK3(365-721) (C-terminus)

have been described (Julien et al., 2003). pEGFP-C2-SVIL was generously provided by Elisabeth Luna (University of Massachusetts Medical School). H2B-mRFP (LV-RFP) was a gift from Elaine Fuchs (Addgene plasmid # 26001) (Beronja et al., 2010). Citrine-α-tubulin 1B was a gift from Guy Sauvageau (Université de Montréal). Plasmid pcDNA3-Flag-SVIL was generated by subcloning SVIL isoform 4 cDNA from pEGFP-C2-SVIL into pcDNA3-Flag vector by Gibson assembly. pcDNA3-Flag and pEGFP-C2 vectors expressing SVIL S245A and S245D mutants were generated by site-directed mutagenesis using mutated primers and Phusion high-fidelity polymerase from New England Biolabs (cat# M0530S). All mutations and PCR products were verified by DNA sequencing.

Commercial antibodies were obtained from the following suppliers: anti-phospho-MAPK motif pPXS*P (1/1000; cat# 2325), Alexa488 anti-Myc tag (1/1000; cat# 2279), anti-phospho-histone H3(S10) (1/200; cat# 9706) from Cell Signaling Technology; anti-ERK3 (1/1000; cat# ab53277 and GTX84146), anti-phospho-MLC(S20) (1/200; cat# ab2480) from Abcam; anti-SVIL (1/500; cat# sc-53556), anti-Myc (1/1000, cat# sc-40), anti-Hsc70 (1/2000; cat# sc-7298), anti-cyclin A (1/1000, cat# sc-596) from Santa-Cruz Biotechnology; anti-Flag (1/1000 for immunoblotting; cat# F3165), anti-Flag (1/100 for immunofluorescence; cat# F1804), anti-α-tubulin (1/10,000; cat# T6199), anti-CDK1 (1/2000; cat# 06-923) from Sigma-Aldrich; Alexa Fluor 555 Phalloidin (1/40; cat# A34055), Alexa Fluor 647 Phalloidin (1/40; cat# A22287), IgG isotype control (cat# 10500C) from ThermoFisher. The phospho-SVIL(S245) and pan-SVIL antibodies were generated by GenScript by immunizing rabbits with the synthetic phospho-peptide EVPR(pS)PEEEERRRVRC coupled to KLH. The antibodies were purified by affinity chromatography. Anti-phospho-SVIL(S245) was used at 1/500 for immunoblotting and 1/50 for immunofluorescence. The anti-pan-SVIL was used at 1/1000 for immunoblotting and 1/200 for immunofluorescence.

Cell lines, cell culture and transfections

Hs578T (*TP53* V157F), MDA-MB-231 (*TP53* R280K) and HEK 293T cells were obtained from the American Type Culture Collection. Hs578T and MDA-MB-231 cell lines were recently authenticated by short tandem repeat profiling (ATCC). Hs578T cell pools depleted of ERK3 or SVIL by CRISPR/Cas9 gene editing were purchased from Synthego. The edited cell populations were generated by electroporation of Hs578T cells with SpCas9 and sgRNA delivered as ribonucleoproteins. The sgRNA sequences used were: *MAPK6*, "UUUGAGAUUCUUGGUCCCAG"; and SVIL, "GCUGGCUCUCAUGUAUCGAG". Gene edition was confirmed by DNA sequencing using Synthego's Inference of CRISPR Edits software. The editing efficiency after expansion of the cell pools was 78% for *MAPK6* and 97% for *SVIL*. All cell lines were cultured in DMEM supplemented with 10% foetal bovine serum and antibiotics at 37°C. Primary mouse embryonic fibroblasts (MEFs) were isolated from ERK3-deficient mice and wild type littermates as previously described (Voisin et al., 2010). The cells were grown in DMEM supplemented with 10% newborn calf serum and antibiotics. For plasmid transfections, HEK 293T cells were transiently transfected with polyethylenimine. Other cell lines were transfected using Lipofectamine 3000 (Invitrogen) according to the manufacturer's protocol.

Cell synchronization

Hs578T cells were plated at a density of 8 x10^5 cells per 10-cm dish for 24 h. The cells were synchronized in S phase by addition of 2 mM thymidine for 22 h. For synchronization in G2 phase, thymidine-treated cells were released for 6 h and treated with 10 μM RO-3306 for 3 h. For synchronization in M phase, thymidine-treated cells were released for 6 h, treated with 50 μg/ml nocodazole for 4 h, followed by treatment with 10 μM MG-132 for 2 h. The cells

were washed three times before each treatment. For synchronization in G1 phase, the cells were serum-starved for 24 h.

RNA interference

For RNAi-mediated silencing of ERK3 or SVIL, the following siRNAs (Horizon Discovery) were used: siNT ON-TARGETplus Cyclophilin B Control (D-001810-10-20), ON-TARGETplus MAPK6 SMARTPool siRNAs (L-003594), Accell MAPK6 individual 3'UTR siRNA #20 (A-003594-20), Accell MAPK6 individual 3'UTR siRNA #21 (A-003594-21), Accell MAPK6 individual siRNA #22 (A-003594-22) and ON-TARGETplus SVIL individual siRNA #5 (J-011398-05). For siRNA transfections, the cells were transfected with RNAiMAX (Invitrogen) according to the manufacturer's instructions.

SILAC and sample preparation

Hs578T cells were cultured for 6 passages in SILAC DMEM medium (ThermoFisher cat# 89985) supplemented with 10% dialyzed FBS (Thermofischer cat# 26400044), proline 870 µM, (Sigma, cat# 81709) and either "light" (Lys(0) 640 µM and Arg(0) 380 µM) or "heavy" (Lys(8) 640 µM and Arg(10) 380 µM) amino acids (Silantes cat# 211603902 and 201603902). Full incorporation of isotopically labeled amino acids was confirmed by analyzing an aliquot of cell extracts by MS after 3 doublings. Light and heavy cell populations (4 biological replicates) were transfected with non-target siRNA or *MAPK6* SmartPool siRNAs for 24 h.

The cells were scraped directly in the culture media, and light and heavy SILAC cultures were combined at this point. Cell pellets were washed several times in cold phosphate-buffered saline (PBS) and subsequently lysed in hypotonic buffer (10 mM NaCl, 10 mM Tris-HCl (pH 7.4), 3 mM $MgCl_2$, 10% (v/v) glycerol and 0.3% (v/v) NP-40) containing protease and phosphatase inhibitors. Lysates were centrifuged at 500 x g for 5 min, and the supernatants

(cytosol) were transferred to new tubes. Proteins from cytosolic fractions were precipitated by MeOH/CHCl3. The pellets (nuclei) were washed in isotonic buffer (8.5 g sucrose/100 mL, 10 mM Tris-HCl (pH 7.4) and 5 mM $MgCl_2$). The proteins were solubilized in digestion buffer (1% sodium deoxycholate, 100 mM Tris-HCl (pH 8.5), 40 mM chloroacetamide and 10 mM TCEP) and incubated at 95°C for 5 min, followed by overnight digestion with trypsin at 37°C (protein:enzyme mass ratio 100:1). Digestion was halted by acidification with formic acid (FA) (final concentration of 0.5%) and the peptides were desalted and concentrated on tC18 Sep-Pak cartridges (Waters) according to the manufacturer's protocol.

MS analysis of phosphopeptides

Phosphopeptide enrichment was performed using TiO2beads as described(Kanshin et al., 2013). Sample loading, washing and elution steps were performed using custom spin columns made from 200-µl pipette tip containing a SDB-XC membrane (3M) frit and filled with TiO_2 beads. The TiO_2 resin was equilibrated in 250 mM lactic acid in 70% acetonitrile (ACN) and 3% TFA, and the same buffer was used for sample loading. Phosphopeptides were eluted from TiO_2 beads with 500 mM phosphate buffer (pH 7.0). Peptides were desalted in 50 µl of 1% FA and subsequently eluted from spin columns using 50 µl of 50% ACN and 0.5% FA. Eluates were dried in a SpeedVac and the phosphopeptides were resuspended in 15 µl of 4% FA prior to MS analysis. MS analysis was performed on a Tribrid Orbitrap Fusion coupled to a Proxeon nanoflow HPLC system. Each sample was loaded on a reverse-phase precolumn (5 mm length, 360 µm i.d.) and separated on a reverse-phase analytical column (18 cm length, 150 µm i.d.) (Jupiter C18, 3 µm, 300 Å, Phenomenex). LC separations were performed at a flow rate of 0.6 µl/min using a linear gradient of 5–40% aqueous ACN (0.2% FA) in 120 min. MS spectra were acquired with a resolution of 70,000 using a lock mass (m/z: 445.120025) followed by up to 10 MS/MS data-dependent scans on the most intense ions using high energy

dissociation (HCD). AGC target values for MS and MS/MS scans were set to 1e6 (max fill time 500 ms) and 1e6 (max fill time 120 ms), respectively. The precursor isolation window was set to m/z 2 with a HCD-normalized collision energy of 25. The dynamic exclusion window was set to 30 s.

MS data processing and bioinformatics

MS data were analyzed using MaxQuant(Cox and Mann, 2008; Cox et al., 2011b) software version 1.3.0.3 and searched against the SwissProt subset of the *H. Sapiens* uniprot database (http://www.uniprot.org/). A list of 248 common laboratory contaminants included in MaxQuant was also added to the database as well as reversed versions of all sequences. The enzyme specificity was set to trypsin with a maximum number of missed cleavages set to 2. The precursor mass tolerance was set to 20 ppm for the first search (used for nonlinear mass re-calibration(Cox et al., 2011a)) and then to 6 ppm for the main search. Phosphorylation of serine, threonine and tyrosine residues was searched as variable modification; carbamidomethylation of cysteines was searched as a fixed modification. The false discovery rate (FDR) for peptide, protein and site identification was set to 1%, the minimum peptide length was set to 6, and the "peptide requantification" function was enabled. The option match between runs (1 min time tolerance after the alignment) was enabled to correlate identification and quantitation results across different runs.

Phosphorylation sites with a decrease in abundance of ≥ 1.2-fold upon ERK3 depletion and an associated t-test *P* value < 0.05 were qualified as ERK3 sensitive. To select for candidate ERK3 substrates, phosphopeptides were further filtered for the presence of the minimal MAP kinase consensus motif Ser/Thr-Pro. GO term analysis was performed using the STRING database. PhosphoLogo analysis(GE et al., 2004) was performed using the WebLogo application (weblogo.berkeley.edu) with standard settings.

In vitro phosphorylation assays

Human recombinant active ERK3 and ERK4 were expressed in Sf9 insect cells from a baculovirus vector and purified as described(Seternes et al., 2004; Perander et al., 2008). Recombinant MK5 was produced as described previously(Déleris et al., 2008). Human SVIL protein was purified from HEK 293T cells transfected with pcDNA3-Flag-SVIL. Proteins were extracted in RIPA lysis buffer (50 mM Tris-HCl (pH 7.4), 150 nM NaCl, 1 mM EDTA, 1% Triton, 0.1% SDS), briefly sonicated, and subjected to immunoprecipitation with anti-Flag antibody overnight at 4^0C. The purity and protein concentration of SVIL was determined by SDS-gel electrophoresis and Coomassie staining. The purified SVIL was then dephosphorylated by incubation with Lambda phosphatase for 30 min at 30°C according to manufacturer's protocol, followed by phosphatase inactivation for 1 h at 65°C. For *in vitro* phosphorylation assays, 5 µg of purified SVIL, MK5, MBP or histone H1 was incubated with either 0.2-1 µg of ERK3, 0.9 µg of ERK4, 25 ng of ERK1 or 100 ng of CDK1/cyclin B1 in kinase buffer (50 mM Tris-HCl (pH 7.4), 10 mM $MgCl_2$, 2 mM dithiothreitol, 0.01% Brij 35, 100 µM ATP and 5 µCi of [γ^{32}P]ATP) for 30 min at 30°C. Proteins were resolved by SDS-gel electrophoresis and SVIL phosphorylation was analyzed by autoradiography and quantified by Cerenkov counting (Tricarb 2800, Perkin-Elmer). Non-radioactive phosphorylation assays were performed in the absence of radioactive ATP and analyzed by immunoblotting with anti-phospho-MAP kinase motif or anti-phospho-SVIL(S245) antibodies. For mapping of SVIL phosphorylation sites by MS, 20 µg of purified SVIL was incubated with 1 µg of active ERK3 in kinase buffer for 2 h at 30°C.

Immunoblot analysis and immunoprecipitation

Proteins were extracted in RIPA lysis buffer supplemented with protease and phosphatase inhibitors with brief sonication. Immunoblotting analysis was performed as described (Servant et al., 2000). For immunoprecipitation, proteins were extracted in Tris lysis buffer (50 mM Tris-HCl (pH 7.4), 250 mM NaCl, 5 mM EDTA, 0.5% NP-40, 10 mM NaF) or RIPA buffer and incubated overnight with indicated antibodies and Protein A or G magnetic beads (Bio-Rad Laboratories).

RNA extraction and quantitative real-time PCR

Total RNA was extracted with the RNeasy Mini Kit (Qiagen) and reverse transcribed with random primers and the High Capacity cDNA Archive Kit (Applied Biosystems) as described by the manufacturer. Quantitative real-time PCR was performed as previously described (Voisin et al., 2010). The threshold cycle (Ct) value for each gene was normalised to the Ct value of actin and GAPDH and the relative levels of expression were calculated.

Quantification of multinucleated cells

For quantification of multinucleated cells, the cells were plated on glass coverslips and transfected as described in figure legends. Then, the cells were fixed with 4% paraformaldehyde for 10 min and washed three times in PBS. The cells were blocked and permeabilized by incubation in 0.1% Triton X-100, 5% bovine serum albumin for 15 min at room temperature (RT). For staining of F-actin, the cells were incubated with Alexa Fluor 555 Phalloidin for 1 h. Nuclei were stained with DAPI for 5 min and the slides were mounted with Mowiol mounting medium. Images were analyzed on an Axio Imager (Zeiss) microscope. At least 1,000 cells/condition were counted in each experiment.

Indirect immunofluorescence and quantitative analysis

Hs578T cells cultured on glass coverslips were transfected using Lipofectamine 3000 and stained 48 h after plating. For staining of MEFs, the cells were directly plated on glass coverslips and stained the next day. The cells were fixed in 4% paraformaldehyde for 5 min at RT, washed three times in PBS, and permeabilized in 0.3 % Triton X-100 in PBS for 5 min at RT. After blocking non-specific sites for 20 min in PBS, 2% BSA, the cells were incubated with primary antibodies diluted in PBS, 0.5% BSA for 1 h at RT. After three washes in PBS, the cells were further incubated with Alexa fluor dyes-conjugated secondary antibodies (1/500) in PBS, 0.5% BSA for 1 h at RT. After three additional washes in PBS, coverslips were treated with a solution of Hoechst 33342 (1 μg/mL in PBS) for 5 min at RT, followed by two washes in PBS. Cells were mounted/sealed using Prolong Gold and allowed to dry overnight at RT before being imaged. For co-staining with goat anti-GFP, primary and secondary antibodies were added sequentially to diminish background due to nonspecific interactions. For the same reason, mouse anti-Myc Alexa 488 was always added last. Phalloidin Alexa 555 was applied to coverslip with secondary antibodies. Images were acquired with a Zeiss LSM700 laser-scanning confocal microscope, illuminated in multi-track mode with 405, 488, 555, and 639 nm laser lines controlled by Zen software (Zeiss). The cells were visualized with a 40×/1.4 NA Plan-Apochromat oil objective and z-stacks (0.8 μm) sectioning the entire cell were taken for all conditions. Images were processed and analyzed from the original files using ImageJ software. For multinucleation experiment, at least 1,000 cells were quantified in at least three independent biological replicates.

To quantify the fluorescence intensity of GFP from Hs578T cells transiently transfected with different forms of EGFP-SVIL (wild type, S245A or S245D), ImageJ software was used to draw a region defining the whole cell to determine the average fluorescence intensity (a. u.) for three or five consecutive z-slices (sum of the three averages for fixed samples, sum of five averages for live-cell imaging). The average fluorescence intensity (a. u.) of a similar area of

background signal was also quantified for the same z-slices (sum of the averages) and subtracted from the GFP fluorescence intensity signal. To quantify the level of RLC Ser19 phosphorylation at the equator of Hs578T cells, ImageJ software was used to draw a region defining the cell equator (5-7 micron wide) and determine the average fluorescence intensity (a. u.) for three consecutive z-slices (sum of the three averages). These values were ratioed over the average fluorescence intensity (a. u.) of the whole cell, for the same z-slices (sum of the three averages). 7-14 cells were quantified in three independent biological replicates. To quantify the accumulation of EGFP-SVIL at the cell equator, maximal intensity projections of the entire z-stack of images collected in live-cell confocal microscopy were generated using the ImageJ software. A 15 micron-thick line was drawn through the equator (i.e. where the furrowing of the contractile ring occurred) of both daughter cells to generate the integrated intensity of fluorescence (a. u.) along these lines. The values of the peaks of fluorescence at the equator (5 consecutive pixels corresponding to the cell cortex) was averaged and rationed over the average of three 5-pixels regions of the cytosolic fluorescence (define as the region in the middle of the line).

Time-lapse confocal microscopy

Hs578T cells were plated on 35-mm microscopy dishes (MatTek Corporation, cat# PG35G-1.5-14-C) and left to adhere overnight before co-transfection with H2B-mRFP and GFP alone or GFP-SVIL wild type, S245A or S245D using Lipofectamine 3000. After 48 h, asynchronous cells in prometaphase were selected and images were collected every 8 min for 18 h by live-cell microscopy at 37°C on a Zeiss LSM700 laser-scanning confocal microscope illuminated in single-track mode with 488 and 555 nm laser lines, controlled by Zen software. Cells were visualized with a 40×/1.4 NA Plan-Apochromat oil objective and z-stacks (0.8 μm) sectioning the entire cell were taken for all conditions. Images were processed and analyzed

from the original files using ImageJ software and presented as maximal intensity projections renderings.

To assess cytokinesis completion or failure, the cells were visualised throughout the entirety of the movie generated by Zen software and scored for “completion” (i.e. complete closure and stabilisation of the contractile ring without reopening) or “failure” (i.e. closure followed by regression of the contractile ring, no furrowing of the ring). Segregation defects were also analysed and cells undergoing multipolar mitosis were excluded. At least 25 cells per condition were imaged and scored.

Statistical analysis

Statistics were analysed using GraphPad Prism 5.0. Pairwise Student t-test was used for comparison of data in paired observations with two unmatched groups. For most of experiments, a one-way ANOVA with Bonferroni post hoc test was used for comparison of data in paired observation experiments containing three unmatched groups or more. For live-cell imaging, a Fisher’s exact test was applied to the different comparisons. For cell ploidy determination in ERK3- or SVIL deleted Hs578T, we applied a two-way ANOVA followed by a post hoc Dunnett’s test. Assumptions of normality and equal variance were met for the data analyzed. In all cases, a two-tailed P value < 0.05 was considered significant. All results are expressed as average ± SEM. In all figures, P values are represented as follow: *P <0 .05, **P < 0.01, ***$P < 0.001$, and n.s. not significant.

Data availability

The mass spectrometry proteomics data have been deposited to the ProteomeXchange Consortium via the PRIDE partner repository with the dataset identifier PXD028061. All other

data generated during this study are included in the main text or supplementary material or are available from the authors on reasonable request.

RESULTS

Quantitative phosphoproteomic analysis identifies SVIL as a candidate ERK3 substrate

We performed quantitative phosphoproteomics analyses using stable isotope labeling by amino acids in cell culture (SILAC)-based phosphoproteomics to uncover novel substrates of ERK3. Exponentially proliferating Hs578T breast cancer cells were labeled with either light or heavy amino acids and depleted or not of ERK3 by short-term treatment with pooled *MAPK6* siRNAs. ERK3 expression was efficiently silenced by RNAi (Fig. 1A). Lysates from differentially labeled cells were combined and, after cellular fractionation, proteins were digested with trypsin and phosphopeptides were enriched using TiO_2 beads. For phosphoproteomic analysis, peptides were separated by reverse-phase chromatography and analyzed by liquid chromatography-tandem mass spectrometry (LC-MS/MS). Overall, we identified 6,760 unique phosphorylation sites on 2,442 proteins from 4 biological replicate experiments (Table S1).

To identify potential ERK3 substrate candidates, we first selected phosphosites whose abundance upon ERK3 depletion was decreased by ≥ 1.2-fold with an associated *t*-test *P* value < 0.05. This produced a list of 50 phosphosites corresponding to a total of 38 distinct proteins (Fig. 1B; Table S2). From this list, we used the PhosphoLogo computational tool to predict a consensus phospho-acceptor motif for ERK3. This analysis revealed that ERK3-regulated phosphoproteins show a clear preference for a proline residue at the +1 position and, to a lesser extent, at the -2 position (Fig. 1C; Table S2), in agreement with the minimal and optimal consensus phosphorylation motifs Ser/Thr-Pro and Pro-Xxx-Ser/Thr-Pro defined for MAP kinases (Gonzalez et al., 1991; Songyang et al., 1996). Gene ontology (GO) analysis of cellular

components revealed that ERK3-regulated phospho-Ser/Thr-Pro proteins are enriched in the cytoskeleton and midbody categories (Table 1). One candidate substrate of special interest was the F-actin- and myosin II-binding protein SVIL. The phosphorylation of multiple SVIL residues was significantly decreased in ERK3-depleted Hs578T cells (Fig. 1B, D, E). We focused our subsequent analysis on the regulation of SVIL Ser245, as this residue lies in an optimal MAP kinase consensus motif.

ERK3 interacts with and phosphorylates SVIL on Ser245

As a first validation step, we tested the ability of ERK3 to phosphorylate SVIL *in vitro*. SVIL is a large protein of ~ 250 kDa that is not easily amenable to purification in bacteria. We therefore expressed full-length human SVIL as a Flag-tagged recombinant protein in HEK 293T cells and purified the protein to > 80% purity by affinity pull-down with anti-Flag M2 magnetic beads. Coomassie staining of the resulting gel revealed the presence of two major bands. The upper band was identified as SVIL isoform 4 by MS, while the lower band corresponded to a mix of SVIL isoform 1 and co-purifying myosin IX and myosin X proteins (Fig. 2A). For *in vitro* phosphorylation assays, purified SVIL was first dephosphorylated with Lambda phosphatase, and then incubated with purified recombinant active ERK3 and ATP. We found that ERK3 phosphorylates SVIL *in vitro* in a dose-dependent manner (Fig. 2A, B) and to an extent comparable to MK5, used as positive control (Fig. 2C). To evaluate the kinase selectivity of SVIL phosphorylation, we further examined the ability of the paralogous ERK4 and the multifunctional ERK1 MAP kinases to phosphorylate SVIL *in vitro*. The amount of each kinase used in the phosphorylation assay was normalized to their enzymatic activity on the common substrate MBP. Interestingly, purified recombinant ERK4 phosphorylated SVIL with an activity comparable to ERK3 (Fig. 2D). However, active ERK1 failed to detectably phosphorylate SVIL, despite the presence of 17 Ser/Thr-Pro motifs in the protein. This indicates

that SVIL is preferentially phosphorylated by the atypical ERK3/ERK4 MAP kinases compared to the classical ERK1 MAP kinase.

MS analysis identified Ser245 as a major *in vitro* phosphorylation site of SVIL by ERK3 (Fig. 2E). Ser245 is one of the most frequently phosphorylated sites of SVIL recorded in the PhosphoSitePlus database (www.phosphosite.org). This site is well conserved among the different SVIL isoforms and across other mammalian species (Fig. 2F). We generated a phospho-specific antibody against SVIL Ser245 to explore the regulation and functional impact of this modification. The phospho-SVIL(S245) antibody strongly reacted with ERK3-phosphorylated immunopurified SVIL, and the immunoreactivity was completely abolished after substitution of Ser245 by Ala or by treatment with Lambda phosphatase, confirming the specificity of the antibody for phosphorylated Ser245 (Fig. 2G).

To substantiate these results, we evaluated if ERK3 phosphorylates SVIL on Ser245 in intact cells. We first examined if ERK3 can co-immunoprecipitate with SVIL. We showed that ERK3 and SVIL form stable complexes when the two proteins are ectopically expressed in HEK 293T cells (Fig. 3A). The two endogenous ERK3 and SVIL proteins were also found to co-immunoprecipitate from Hs578T cell extracts (Fig. 3B). Co-expressing the individual domains of ERK3 with SVIL in HEK 293T revealed that SVIL preferentially interacts with the ERK3(365-721) C-terminal domain (Fig. 3C). We used the phospho-SVIL(S245) antibody to assess if changes in ERK3 levels impact SVIL Ser245 phosphorylation *in vivo*. Co-expression of ERK3 with SVIL in HEK 293T cells significantly increased the phosphorylation of SVIL on Ser245, and this signal was completely abolished when expressing the non-phosphorylatable SVIL S245A mutant (Fig. 3D). Similar result were obtained after probing extracts with a phospho-MAP kinase motif antibody (Fig. 3D). RNAi-mediated depletion of ERK3 significantly decreased (but did not eliminate) the steady-state phosphorylation of SVIL on

Ser245 (Fig. 3E). Together, these results identify SVIL as a novel *bona fide* ERK3 substrate and Ser245 as a major site of ERK3 activity.

ERK3 regulates cell ploidy through phosphorylation of SVIL on Ser245

SVIL is a member of the large family of gelsolin/villin proteins and was shown to regulate various properties of the cell cortex, in part through direct binding to F-actin and myosin II via its N-terminal region. One important activity of SVIL, demonstrated in HeLa cells, is to contribute to the proper initiation and completion of cytokinesis, thus ensuring the separation of chromosomes into distinct daughter cells at the end of mitosis (Smith et al., 2010, 2013; Hasegawa et al., 2013). We therefore asked whether phosphorylation of SVIL on Ser245 by ERK3 impacts cytokinesis. We first used immunofluorescence to assess whether RNAi-mediated depletion of ERK3 or SVIL in breast cancer cell lines resulted in an increase in the proportion of multinucleated cells, a typical consequence of cytokinetic failure. We found that transient depletion of ERK3 with three distinct siRNAs led to a small but significant increase in the proportion of multinucleated Hs578T cells (Fig. S1A-C). Consistent with previous reports (Smith et al., 2010, 2013; Hasegawa et al., 2013), RNAi depletion of SVIL also increased the percentage of multinucleated Hs578T cells compared to control (Fig. S1A-C). The percentage of multinucleated SVIL-depleted cells was smaller than observed previously in HeLa cells (Hasegawa et al., 2013), which could be due to cell type differences. Interestingly, re-expression of either wild type or phosphomimetic S245D forms of SVIL in SVIL-depleted cells significantly rescued the frequency of multinucleated cells to a degree comparable to controls, while expression of the non-phosphorylatable S245A mutant had no such effect (Fig. S1A-C). Comparable results were obtained with the breast cancer cell line MDA-MB-231 (Fig. S1D-F), indicating that the impact of ERK3 and SVIL activity on cell ploidy is not specific to Hs578T cells.

We employed a pharmacological approach to further validate the impact of ERK3 on SVIL phosphorylation and cell ploidy. Treatment of Hs578T cells with a small molecule inihibitor of ERK3 (Grädler et al., 2020) reduced the phosphorylation of SVIL on Ser245 (Fig. 4A). Furthermore, pharmacological inhibition of ERK3 significantly increased the frequency of multinucleated Hs578T cells (Fig. 4B, C), demonstrating the requirement for the catalytic activity of ERK3 and providing orthogonal validation to the genetic depletion experiments). Treatment with ERK3 inhibitor did not further increase the multinucleation of SVIL-depleted cells (Fig. 4B; see also Fig. 5A), suggesting that ERK3 and SVIL lie on the same signaling axis. These results demonstrate that both ERK3 and SVIL are required to maintain proper cell ploidy and suggest that phosphorylation of SVIL at Ser245 is functionally relevant for cell division. Of note, no difference in cell ploidy was observed between wild type and ERK3-deficient primary MEFs (Fig. S2), suggesting that this regulation may be context-dependent (see Discussion).

To further demonstrate that ERK3 and SVIL function together to regulate cell ploidy, we used CRISPR/Cas9-mediated gene editing to generate Hs578T cells depleted of either gene product. The knockdown efficiency was estimated to be ~ 90% for ERK3 and > 80% for SVIL (Fig. 5A). While ERK3- or SVIL-depleted Hs578T cells were viable, they showed an increase in the percentage of multinucleated cells compared to control Hs578T cells (Fig. 5B, C), consistent with the results obtained by RNAi and pharmacological inhibition. Expression of GFP-tagged wild type or phosphomimetic S245D forms of SVIL rescued the multinucleation phenotype associated with SVIL depletion, while expressing the non-phosphorylatable S245A form of SVIL had no such effect (Fig. 5B, C). Notably, expression of wild type or S245D forms of SVIL in ERK3-depleted cells also rescued multinucleation (Fig. 5B, C), consistent with SVIL regulating cell ploidy downstream of ERK3. The observation that overexpression of wild type SVIL can rescue ploidy in ERK3-depleted cells suggests that another kinase (other than

ERK4 that is not expressed in Hs578T cells) can phosphorylate SVIL at Ser245 to compensate for the loss of ERK3. This is in agreement with our finding that RNAi depletion of ERK3 does not completely abolish SVIL Ser245 phosphorylation (see Fig. 3E). CDK1 also preferentially phosphorylates Ser/Thr residues followed by a proline, making it a candidate SVIL kinase. However, we found that CDK1/cyclin B does not phosphorylate SVIL on Ser245 *in vitro* (Fig. S3). Together, our results support the notion that Ser245 phosphorylation of SVIL by ERK3 is functionally relevant for SVIL activity in the regulation of cell division.

ERK3 phosphorylation of SVIL on Ser245 regulates cytokinesis

To determine whether the changes in Hs578T cell ploidy resulting from loss of ERK3 or SVIL were due to defects in cytokinesis, we used time-lapse confocal imaging of dividing control, ERK3- or SVIL-depleted Hs578T cells transiently expressing fluorescent protein-tagged versions of alpha-tubulin and histone H2B to monitor mitotic progression (Movies S1-3). We also transiently co-expressed EGFP-tagged forms of SVIL (wild type, S245A or S245D) with histone H2B in control, ERK3- or SVIL-depleted Hs578T cells to further assay the role of Ser245 in SVIL function. All cell populations were viable and most individual cells monitored entered mitosis. In nearly all cell lines, we observed a small percentage of cells forming multipolar spindles after mitotic entry, consistent with our findings that ploidy is impacted in Hs578T cells and that this defect is exacerbated by loss of SVIL or ERK3; as this multipolar spindle defect likely arises of previous cell division failures, these cells were excluded from subsequent analyses. All other cells that entered mitosis formed a bipolar spindle that elongated normally at anaphase. While most mitoses completed with the formation of two distinct daughter cells, a fraction of the cells underwent cytokinetic failure, ending with a single, binucleated cell (Fig. 6A). In most of these cases, the cytokinetic furrow formed and initiated ingression normally but subsequently regressed. No furrow ingression was observed in a small

proportion of mitotic cells. The frequency of cytokinetic failure significantly increased upon depletion of ERK3 or SVIL (Fig. 6A, B), indicating that both proteins impact cell ploidy via their regulatory effect on cytokinesis. As observed for cell ploidy, cytokinetic defects in ERK3- and SVIL-depleted Hs578T cells were rescued by expressing either the wild type or S245D form of SVIL, but not the non-phosphorylatable S245A mutant (Fig. 6A, C, D). Importantly, measuring the total levels of GFP signal intensity revealed that there was no correlation between the expression levels of the different GFP-fused SVIL constructs and the extent of cytokinesis failure, arguing that the observed cytokinesis rescue arises of SVIL activity rather than level (Fig. 6E). Altogether, these results indicate that phosphorylation of SVIL at Ser245 by ERK3 impacts Hs578T cell ploidy by ensuring proper mitotic progression and completion of cytokinesis.

Phosphorylation of SVIL on Ser245 is upregulated during mitosis

We sought to gain insight into the mechanism by which ERK3 phosphorylation of SVIL regulates cytokinesis completion. We first asked whether ERK3 signaling regulates the expression level of SVIL in the cell. No significant reduction of SVIL mRNA and protein levels was observed after RNAi depletion of ERK3 in Hs578T or MDA-MB-231 breast cancer cells (Fig. S4A-D). In HeLa cells undergoing cytokinesis, SVIL was shown to localize at the leading edge of the ingressing furrow and become enriched at the midbody prior to abscission (Smith et al., 2010, 2013). We used immunofluorescence analysis of Hs578T cells co-expressing epitope-tagged versions of ERK3 and SVIL to assess whether the two proteins colocalize at any time during mitotic progression. While no strong colocalization was observed, we found that the two ectopic proteins transiently accumulated at spindle poles in late anaphase, and SVIL localized at the midbody in telophase (Fig. 7A). Using antibodies specific to ERK3 and SVIL, we found that the two endogenous proteins wealy co-localized at the midbody in telophase (Fig.

7B). The small differences observed between these stainings may result from differences in epitope exposure, yet these results indicate that the two proteins can colocalize to discrete subcellular compartments during mitosis.

To determine whether SVIL is phosphorylated on Ser245 in a cell cycle-dependent manner, Hs578T cells were synchronized at different stages of the cell cycle and the phosphorylation of endogenous SVIL was monitored by immunoblotting. We observed that SVIL Ser245 phosphorylation is markedly upregulated in mitosis, concomitant to the accumulation of ERK3 and SVIL (Fig. 7C). These results are in agreement with our previous study showing the stabilization and accumulation of ERK3 in mitotic cells (Tanguay et al., 2010). Staining of SVIL-depleted Hs578T cells expressing wild type SVIL with the phospho-SVIL(S245) antibody revealed that this signal is enriched at spindle poles during anaphase and at the midbody in late telophase, while this signal is absent in cells reconstituted with SVIL S245A mutant (Fig. 7D). Together, these results support the notion that SVIL Ser245 phosphorylation by ERK3, possibly at or near the spindle pole in late anaphase, promotes the accumulation of phospho-SVIL at the ingressing furrow and midbody in telophase, where it contributes to coordinate the completion of cytokinesis.

ERK3 phosphorylation of SVIL Ser245 regulates activation of myosin II regulatory light chain during cytokinesis

Previous work demonstrated that SVIL regulates cytokinesis in part by controlling the activation of non-muscle myosin II at the cleavage furrow (Hasegawa et al., 2013). Myosin II activation is achieved by phosphorylation of its regulatory light chain (RLC) on Ser19, which is required for constriction of the contractile ring (Asano et al., 2009; Dean and Spudich, 2006; Komatsu et al., 2000). Thus, we hypothesized that the impact of SVIL phosphorylation by ERK3 on cytokinesis execution could be mediated through myosin II RLC phosphorylation and

activation. To test this, we used immunofluorescence to monitor the levels of Ser19-phosphorylated RLC in Hs578T cells undergoing mitosis. We found that Hs578T cells depleted of either ERK3 or SVIL have lower relative levels of myosin II phospho-RLC(S19) at the cell equator during anaphase as compared to control cells (Fig. 8A, B). Notably, the decreased accumulation of Ser19-phosphorylated RLC was rescued by re-expressing the wild type or S245D forms of SVIL, but not SVIL S245A (Fig. 8A, B). No correlation was observed between the expression levels of SVIL S245A rescuing construct and myosin II phospho-RLC(S19) levels in SVIL-depleted Hs578T cells (Fig. 8C). These results indicate that phosphorylation of SVIL at Ser245 contributes to maintaining high levels of Ser19-phosphorylated RLC at the cell equator, suggesting a mechanism by which phosphorylation of SVIL by ERK3 sustains myosin II activation at the cytokinetic ring.

DISCUSSION

The current study increases our understanding of the roles of the atypical MAP kinase ERK3 in cell physiology. Using a SILAC-based quantitative phosphoproteomics approach, we identified several candidate ERK3 substrates and downstream effectors in breast cancer epithelial cells, including the actomyosin scaffold protein SVIL. Using a combination of *in vitro* and *in vivo* assays, we confirmed that ERK3 interacts with and directly phosphorylates SVIL on Ser245. We further demonstrated that this phosphorylation event is functionally important for the sustained activation of non-muscle myosin II at the cleavage furrow and the proper completion of cytokinesis. These findings unveil a molecular mechanism by which the activity of ERK3 impacts cell division and ploidy.

Very little is known about the substrates and downstream effectors of the atypical MAP kinases ERK3 and ERK4, which has considerably hampered the understanding of their biological functions. No large-scale analysis of the ERK3 or ERK4 phosphoproteome has been

reported to date. The first, and still only validated, substrate identified for ERK3 and ERK4 is the protein kinase MK5 (Seternes et al., 2004; Schumacher et al., 2004; Aberg et al., 2006; Kant et al., 2006). ERK3 was also reported to phosphorylate steroid receptor coactivator-3 (SRC-3) on Ser857, promoting its interaction with the ETS transcription factor PEA3 and gene expression (Long et al., 2012). However, Ser857 lies in a MK consensus phospho-acceptor motif and a subsequent study has shown that SRC-3 is instead phosphorylated at Ser857 by MK5 (Shrestha et al., 2020). Here, we have used a SILAC-based quantitative phosphoproteomics approach to discover novel substrates and effectors of ERK3. Along with SVIL, our analysis uncovered 37 proteins that show a significant decrease in phosphorylation upon depletion of ERK3 in Hs578T cells, considerably expanding our knowledge of this signaling network. One limitation of our study is that MS analysis was performed at steady-state in proliferating cells depleted of ERK3 by RNAi. Contrary to classical MAP kinases like ERK1/2, ERK3 displays constitutive kinase activity in cells and no upstream activator has been identified so far, which prevents the possibility of acutely stimulating the activity of the kinase. Despite this inherent limitation, the following observations validate our approach and point to new areas of ERK3 biology research. First, PhosphoLogo analysis of ERK3-sensitive phosphoproteins revealed a strong preference for a proline residue at position +1 and -2, in agreement with the consensus phosphorylation motif of the MAP kinase family. Indeed, ERK3 and ERK4 phosphorylate MK5 at Thr182, which is followed by a Pro residue. Second, some ERK3-regulated phosphoproteins, such as septin family members, are already known to be regulated by ERK3-MK5 signaling (Brand et al., 2012; Shiryaev et al., 2012). Third, GO analysis of ERK3-regulated phospho-Ser/Thr-Pro proteins showed an enrichment in the cytoskeleton cellular component, consistent with the known functions of ERK3 in cellular adhesion, migration and invasion. The validation of SVIL as a *bona fide* ERK3 substrate confirms the predictive value of our analysis.

We identified Ser245, which lies in a full MAP kinase consensus motif, as a major SVIL phosphorylation site by ERK3. Notably, the phosphorylation of SVIL on Ser245 has been detected in 76 large-scale proteomic studies (www.phosphosite.org), but the kinase(s) involved in this regulation was not identified. We further showed that SVIL is phosphorylated by the paralogous kinase ERK4, but not by ERK1. ERK3 and ERK4 share a common C34 domain (Coulombe and Meloche, 2007), which is localized in the unique C-terminal extension and is absent from ERK1. The C-terminal extension of ERK3 is highly conserved in vertebrate evolution and was shown to mediate the interaction of ERK3 with its substrate MK5 (Åberg et al., 2009), as well as with other binding proteins such as cyclin D3, Cdc14A and septin 7 (Brand et al., 2012; Sun et al., 2006; Hansen et al., 2008). Similarly, we found that SVIL co-immunoprecipitates with the C-terminal extension of ERK3, which may contribute to the unique substrate selectivity of the atypical MAP kinases ERK3 and ERK4.

Our findings provide strong evidence that ERK3 and SVIL act in a linear pathway to regulate cytokinesis execution, unveiling a new cellular function of the poorly characterized MAP kinase ERK3 in cell division. We observed that Ser245-phosphorylated SVIL accumulates at the midbody, pointing to a role of ERK3 in controlling the localization of SVIL to coordinate cytokinesis execution. Mechanistically, we showed that phosphorylation of SVIL Ser245 by ERK3 is necessary to maintain high levels of Ser19-phosphorylated RLC at the cleavage furrow, suggesting that ERK3 signaling may regulate cytokinesis execution by promoting myosin II activation. Phosphorylation of RLC Ser19 by Rho-dependent kinases is required for the activation of myosin II at the cleavage furrow and the generation of inward contractile force driving furrow ingression and cell division (Matsumura, 2005). Further studies are needed to delineate the precise mechanism by which ERK3-mediated phosphorylation of SVIL is linked to myosin II activation at the cortex during cytokinesis. Moreover, we do not

exclude the possibility that SVIL phosphorylation by ERK3 may impact other actin-driven cellular functions of SVIL.

Is is noteworthy that the loss of ERK3 did not increase the frequency of multinucleated cells in primary MEFs. One possible explanation is that ERK4, which is weakly expressed in MEFs (Rousseau et al., 2010), can compensate for the loss of ERK3. An alternative possibility is that the impact of ERK3 inactivation is dependent on the cellular context and becomes manifest in cancer cells, which exhibit a variety of genetic instability phenotypes and are prone to cell division errors. There is evidence that ERK3 signaling sustains the proliferation, anchorage-independent growth, and tumorigenesis of lung and breast cancer cells (Cai et al., 2021). Inactivation of ERK3 in some cancer cells may increase the rate of cell division errors leading to a decrease in cellular fitness and long-term cell proliferation by mechanisms that remain to be investigated.

ACKNOWLEDGMENTS

We thank Éric Bonneil for MS analysis and Joël Flynn-Robitalille for synthesis of the ERK3 inhibitor. Proteomics analyses were performed by the Center for Advanced Proteomics Analyses, a Node of the Canadian Genomic Innovation Network that is supported by the Canadian Government through Genome Canada. J.J. is recipient of fellowships from the Fonds de recherche du Québec Santé and Power Corporation of Canada. This work was supported by grants from the Canadian Institutes for Health Research (PJT-152911) and the Cancer Research Society (25388) to S.M., the Natural Sciences and Engineering Research Council to P.T. (311598), the Cancer Research Society (24475) to J.C.L., and the Norwegian Cancer Society (198119) and North Norwegian Health Authorities (HNF-1547-20) to O.M.S.

AUTHOR CONTRIBUTIONS

J.J. and S.M. designed the project and wrote the manuscript. J.J., E.G., E.K. and M.S. performed and analysed most experiments. A.B. contributed to phosphorylation assays. O.M.S. provided the purified ERK3 and ERK4 kinases. J.J. wrote the initial draft. E.G., J.C.L. and P.T. critically reviewed the experimental data and revised the manuscript. All authors commented on and approved the manuscript.

CONFLICT OF INTEREST

The authors declare no competing interests.

REFERENCES

Åberg, E., M. Perander, B. Johansen, C. Julien, S. Meloche, S.M. Keyse, and O.M. Seternes. 2006. Regulation of MAPK-activated protein kinase 5 activity and subcellular localization by the atypical MAPK ERK4/MAPK4. *J. Biol. Chem.* 281: 35499–35510.

Åberg, E., K.M. Torgersen, B. Johansen, S.M. Keyse, M. Perander, and O.M. Seternes. 2009. Docking of PRAK/MK5 to the atypical MAPKs ERK3 and ERK4 defines a novel MAPK interaction motif. *J. Biol. Chem.* 284:19392–19401.

Al-Mahdi, R., N. Babteen, K. Thillai, M. Holt, B. Johansen, H.L. Wetting, O.M. Seternes, and C.M. Wells. 2015. A novel role for atypical MAPK kinase ERK3 in regulating breast cancer cell morphology and migration. *Cell Adhes. Migr.* 9:483–494.

Asano, S., K. Hamao, and H. Hosoya. 2009. Direct evidence for roles of phosphorylated regulatory light chain of myosin II in furrow ingression during cytokinesis in HeLa cells. *Genes to Cells*. 14:555–568.

Beronja, S., G. Livshits, S. Williams, and E. Fuchs. 2010. Rapid functional dissection of genetic networks via tissue-specific transduction and RNAi in mouse embryos. *Nat. Med.* 16:821–827.

Bhuwania, R., S. Cornfine, Z. Fang, M. Krüger, E.J. Luna, and S. Linder. 2012. Supervillin couples myosin-dependent contractility to podosomes and enables their turnover. *J. Cell Sci.* 125:2300–2314.

Bogucka, K., M. Pompaiah, F. Marini, H. Binder, G. Harms, M. Kaulich, M. Klein, C. Michel, M.P. Radsak, S. Rosigkeit, P. Grimminger, H. Schild, and K. Rajalingam. 2020. ERK3/MAPK6 controls IL-8 production and chemotaxis. *Elife*. 9:e52511.

Brand, F., S. Schumacher, S. Kant, M.B. Menon, R. Simon, B. Turgeon, S. Britsch, S. Meloche, M. Gaestel, and A. Kotlyarov. 2012. The extracellular signal-regulated kinase 3 (Mitogen-Activated Protein Kinase 6 [MAPK6])–MAPK-activated protein kinase 5 signaling complex regulates septin function and dendrite morphology. *Mol. Cell. Biol.* 32: 2467–2478.

Cai, Q., W. Zhou, W. Wang, B. Dong, D. Han, T. Shen, C.J. Creighton, D.D. Moore, and F. Yang. 2021. MAPK6-AKT signaling promotes tumor growth and resistance to mTOR kinase blockade. *Sci. Adv*. 7:eabi6439.

Cargnello, M., and P.P. Roux. 2011. Activation and function of the MAPKs and their substrates, the MAPK-activated protein kinases. *Microbiol. Mol. Biol. Rev.* 75:50–83.

Cheng, M., T.G. Boulton, and M.H. Cobb. 1996. ERK3 is a constitutively nuclear protein kinase. *J. Biol. Chem.* 271:8951–8958.

Coulombe, P., and S. Meloche. 2007. Atypical mitogen-activated protein kinases: Structure, regulation and functions. *Biochim. Biophys. Acta.* 1773:1376–1387.

Coulombe, P., G. Rodier, S. Pelletier, J. Pellerin, and S. Meloche. 2003. Rapid turnover of extracellular signal-regulated kinase 3 by the ubiquitin-proteasome pathway defines a novel paradigm of mitogen-activated protein kinase regulation during cellular differentiation. *Mol. Cell. Biol.* 23:4542–4558.

Cox, J., and M. Mann. 2008. MaxQuant enables high peptide identification rates, individualized

p.p.b.-range mass accuracies and proteome-wide protein quantification. *Nat. Biotechnol.* 26:1367–1372.

Cox, J., A. Michalski, and M. Mann. 2011a. Software lock mass by two-dimensional minimization of peptide mass errors. *J. Am. Soc. Mass Spectrom.* 22:1373–1380.

Cox, J., N. Neuhauser, A. Michalski, R.A. Scheltema, J. V. Olsen, and M. Mann. 2011b. Andromeda: A peptide search engine integrated into the MaxQuant environment. *J. Proteome Res.* 10:1794–1805.

Crowley, J.L., T.C. Smith, Z. Fang, N. Takizawa, and E.J. Luna. 2009. Supervillin reorganizes the actin cytoskeleton and increases invadopodial efficiency. *Mol. Biol. Cell*. 20:948–962.

Dean, S.O., and J.A. Spudich. 2006. Rho Kinase's role in Myosin recruitment to the equatorial cortex of mitotic Drosophila S2 cells is for Myosin regulatory light chain phosphorylation. *PLoS One*. 1:e131.

Déleris, P., L.É. Ris, J. Rousseau, P. Coulombe, G. Genevie`, G. Rodier, P.-L. Tanguay, and S. Meloche. 2008. Activation loop phosphorylation of the atypical MAP kinases ERK3 and ERK4 is required for binding, activation and cytoplasmic relocalization of MK5. *J. Cell. Physiol*. 217:778–788.

Déléris, P., M. Trost, I. Topisirovic, P.L. Tanguay, K.L.B. Borden, P. Thibault, and S. Meloche. 2011. Activation loop phosphorylation of ERK3/ERK4 by group I p21-activated kinases (PAKs) defines a novel PAK-ERK3/4-MAPK-activated protein kinase 5 signaling pathway. *J. Biol. Chem.* 286:6470–6478.

Elkhadragy, L., M. Chen, K. Miller, M.H. Yang, and W. Long. 2017. A regulatory BMI1/let-7i/ERK3 pathway controls the motility of head and neck cancer cells. *Mol. Oncol.* 11:194–207.

Fang, Z., N. Takizawa, K.A. Wilson, T.C. Smith, A. Delprato, M.W. Davidson, D.G. Lambright, and E.J. Luna. 2010. The membrane-associated protein, Supervillin,

accelerates F-actin-dependent rapid integrin recycling and cell motility. *Traffic*. 11:782–799.

GE, C., H. G, C. JM, and B. SE. 2004. WebLogo: a sequence logo generator. *Genome Res.* 14:1188–1190.

Gonzalez, F.A., D.L. Raden, and R.J. Davis. 1991. Identification of substrate recognition determinants for human ERK1 and ERK2 protein kinases. *J. Biol. Chem.* 266:22159–22163.

Grädler, U., M. Busch, B. Leuthner, M. Raba, L. Burgdorf, M. Lehmann, N. Linde, and C. Esdar. 2020. Biochemical, cellular and structural characterization of novel and selective ERK3 inhibitors. Bioorg. Med. Chem. Lett. 30: 127551.

Hansen, C.A., J. Bartek, and S. Jensen. 2008. A functional link between the human cell cycle-regulatory phosphatase Cdc14A and the atypical mitogen-activated kinase Erk3. *Cell Cycle* 7: 325–334.

Hasegawa, H., T. Hyodo, E. Asano, S. Ito, M. Maeda, H. Kuribayashi, A. Natsume, T. Wakabayashi, M. Hamaguchi, and T. Senga. 2013. The role of PLK1-phosphorylated SVIL in myosin II activation and cytokinetic furrowing. *J. Cell Sci.* 126:3627–3637.

Julien, C., P. Coulombe, and S. Meloche. 2003. Nuclear export of ERK3 by a CRM1-dependent mechanism regulates its inhibitory action on cell cycle progression. *J. Biol. Chem.* 278:42615–42624.

Kanshin, E., S.W. Michnick, and P. Thibault. 2013. Displacement of N/Q-rich peptides on TiO2 beads enhances the depth and coverage of yeast phosphoproteome analyses. *J. Proteome Res.* 12:2905–2913.

Kant, S., S. Schumacher, M.K. Singh, A. Kispert, A. Kotlyarov, and M. Gaestel. 2006. Characterization of the atypical MAPK ERK4 and its activation of the MAPK-activated protein kinase MK5. *J. Biol. Chem.* 281: 35511–35519.

Komatsu, S., T. Yano, M. Shibata, R.A. Tuft, and M. Ikebe. 2000. Effects of the regulatory light chain phosphorylation of myosin II on mitosis and cytokinesis of mammalian cells. *J. Biol. Chem.* 275:34512–34520.

De La Mota-Peynado, A., J. Chernoff, and A. Beeser. 2011. Identification of the atypical MAPK Erk3 as a novel substrate for p21-activated Kinase (Pak) activity. *J. Biol. Chem.* 286:13603–13611.

Long, W., C.E. Foulds, J. Qin, J. Liu, C. Ding, D.M. Lonard, L.M. Solis, I.I. Wistuba, J. Qin, S.Y. Tsai, M.J. Tsai, and B.W. O'Malley. 2012. ERK3 signals through SRC-3 coactivator to promote human lung cancer cell invasion. *J. Clin. Invest.* 122:1869–1880.

Mathien, S., P. Déléris, M. Soulez, L. Voisin, and S. Meloche. 2017. Deubiquitinating enzyme USP20 regulates extracellular signal-regulated kinase 3 stability and biological activity. *Mol. Cell. Biol.* 37:e00432-16.

F. Matsumura. 2005. Regulation of myosin II during cytokinesis in higher eukaryotes. *Trends Cell Biol.* 15: 371–377.

Nag, S., M. Larsson, R.C. Robinson, and L.D. Burtnick. 2013. Gelsolin: The tail of a molecular gymnast. *Cytoskeleton*. 70:360–384.

Perander, M., E. Åberg, B. Johansen, B. Dreyer, I.J. Guldvik, H. Outzen, S.M. Keyse, and O.M. Seternes. 2008. The Ser186 phospho-acceptor site within ERK4 is essential for its ability to interact with and activate PRAK/MK5. *Biochem. J.* 411:613–622.

Rousseau, J., S. Klinger, A. Rachalski, B. Turgeon, P. Déléris, E. Vigneault, J.F. Poirier-Héon, M.A. Davoli, N. Mechawar, S. El Mestikawy, N. Cermakian, and S. Meloche. 2010. Targeted inactivation of Mapk4 in mice reveals specific nonredundant functions of Erk3/Erk4 subfamily mitogen-activated protein kinases. *Mol. Cell. Biol*. 30:5752-5763.

Schumacher, S., K. Laass, S. Kant, Y. Shi, A. Visel, A.D. Gruber, A. Kotlyarov, and M. Gaestel. 2004. Scaffolding by ERK3 regulates MK5 in development. *EMBO J.* 23:4770–4779.

Servant, M.J., P. Coulombe, B. Turgeon, and S. Meloche. 2000. Differential regulation of p27(Kip1) expression by mitogenic and hypertrophic factors: Involvement of transcriptional and posttranscriptional mechanisms. *J. Cell Biol.* 148:543–556.

Seternes, O.-M., T. Mikalsen, B. Johansen, E. Michaelsen, C.G. Armstrong, N.A. Morrice, B. Turgeon, S. Meloche, U. Moens, and S.M. Keyse. 2004. Activation of MK5/PRAK by the atypical MAP kinase ERK3 defines a novel signal transduction pathway. *EMBO J.* 23:4780–4791.

Shiryaev, A., S. Kostenko, G. Dumitriu, and U. Moens. 2012. Septin 8 is an interaction partner and in vitro substrate of MK5. *World J. Biol. Chem.* 3: 98-109.

Shrestha, A., H. Bruckmueller, H. Kildalsen, G. Kaur, M. Gaestel, H.L. Wetting, I. Mikkola, and O.-M. Seternes. 2020. Phosphorylation of steroid receptor coactivator-3 (SRC-3) at serine 857 is regulated by the p38MAPK-MK2 axis and affects NF-κB-mediated transcription. *Sci. Rep.* 10: 11388.

Smith, T.C., Z. Fang, and E.J. Luna. 2010. Novel interactors and a role for Supervillin in early cytokinesis. *Cytoskeleton*. 67:346–364.

Smith, T.C., P.C. Fridy, Y. Li, S. Basil, S. Arjun, R.M. Friesen, J. Leszyk, B.T. Chait, M.P. Rout, and E.J. Luna. 2013. Supervillin binding to myosin II and synergism with anillin are required for cytokinesis. *Mol. Biol. Cell*. 24:3603–3619.

Songyang, Z., K.P. Lu, Y.T. Kwon, L.H. Tsai, O. Filhol, C. Cochet, D.A. Brickey, T.R. Soderling, C. Bartleson, D.J. Graves, A.J. DeMaggio, M.F. Hoekstra, J. Blenis, T. Hunter, and L.C. Cantley. 1996. A structural basis for substrate specificities of protein Ser/Thr kinases: primary sequence preference of casein kinases I and II, NIMA, phosphorylase kinase, calmodulin-dependent kinase II, CDK5, and Erk1. *Mol. Cell. Biol.* 16:6486–6493.

Soulez, M., M.K. Saba-El-Leil, B. Turgeon, S. Mathien, P. Coulombe, S. Klinger, J. Rousseau, K. Lévesque, and S. Meloche. 2019. Reevaluation of the role of extracellular signal-

regulated kinase 3 in perinatal survival and postnatal growth using new genetically engineered mouse models. *Mol. Cell. Biol*. 39:e00527-18.

Soulez, M., P.L. Tanguay, F. Dô, J. Dort, C. Crist, A. Kotlyarov, M. Gaestel, M. Ferron, N.A. Dumont, and S. Meloche. 2022. ERK3-MK5 signaling regulates myogenic differentiation and muscle regeneration by promoting FoxO3 degradation. *J. Cell. Physiol*. 237:2271-2287.

Sun, M., Y. Wei, L. Yao, J. Xie, X. Chen, H. Wang, J. Jiang, and J. Gu. 2006. Identification of extracellular signal-regulated kinase 3 as a new interaction partner of cyclin D3. *Biochem. Biophys. Res. Commun.* 340: 209–214.

Takizawa, N., R. Ikebe, M. Ikebe, and E.J. Luna. 2007. Supervillin slows cell spreading by facilitating myosin II activation at the cell periphery. *J. Cell Sci.* 120:3792–3803.

Takizawa, N., T.C. Smith, T. Nebl, J.L. Crowley, S.J. Palmieri, L.M. Lifshitz, A.G. Ehrhardt, L.M. Hoffman, M.C. Beckerle, and E.J. Luna. 2006. Supervillin modulation of focal adhesions involving TRIP6/ZRP-1. *J. Cell Biol.* 174:447–458.

Tanguay, P.L., G. Rodier, and S. Meloche. 2010. C-terminal domain phosphorylation of ERK3 controlled by Cdk1 and Cdc14 regulates its stability in mitosis. *Biochem. J.* 428:103–111.

Tanoue, T., M. Adachi, T. Moriguchi, and E. Nishida. 2000. A conserved docking motif in MAP kinases common to substrates, activators and regulators. *Nat. Cell Biol.* 2:110–116.

Trempolec, N., N. Dave-Coll, and A.R. Nebreda. 2013. SnapShot: P38 MAPK substrates. *Cell*. 152:924-924.e1.

Ünal, E.B., F. Uhlitz, and N. Blüthgen. 2017. A compendium of ERK targets. *FEBS Lett.* 591:2607–2615.

Voisin, L., M.K. Saba-El-Leil, C. Julien, C. Frémin, and S. Meloche. 2010. Genetic demonstration of a redundant role of extracellular signal-regulated kinase 1 (ERK1) and ERK2 mitogen-activated protein kinases in promoting fibroblast proliferation. *Mol. Cell.*

Biol. 30:2918–2932.

Wang, W., K. Bian, S. Vallabhaneni, B. Zhang, R.C. Wu, B.W. O'Malley, and W. Long. 2014. ERK3 promotes endothelial cell functions by upregulating SRC-3/SP1-Mediated VEGFR2 Expression. *J. Cell. Physiol.* 229:1529–1537.

Zeke, A., M. Misheva, A. Reményi, and M.A. Bogoyevitch. 2016. JNK signaling:Regulation and functions based on complex protein-protein partnerships. *Microbiol. Mol. Biol. Rev.* 80:793–835.

FIGURE LEGENDS

Figure 1. Quantitative phosphoproteomic profiling of ERK3 signaling network

(A) Representative immunoblot of ERK3 expression after RNAi-mediated depletion in Hs578T cells. **(B)** Volcano plot of quantitative changes in phosphopeptides in the cytosolic and nuclear fractions of ERK3-depleted Hs578T cells plotted as Log_2 fold-change and *P* value. Phosphopeptides displaying a significant decrease in abundance (fold change ≥ 1.2 and $P < 0.05$, paired *t*-test) are highlighted in red. Data are from 4 biological replicates. **(C)** PhosphoLogo representation of ERK3-sensitive phosphosites. **(D)** SVIL phosphorylation sites showing significant changes (paired Student's *t*-test) upon depletion of ERK3 in Hs578T cells. Data are mean ± SEM (n=4). **(E)** MS/MS spectrum confirming the phosphorylation of SVIL on Ser245.

Figure 2. ERK3 directly phosphorylates SVIL on Ser245 *in vitro*

(A) *In vitro* phosphorylation assay. Immunopurified SVIL was dephosphorylated with Lambda phosphatase prior to incubation with recombinant active ERK3 in the presence of radioactive ATP for 30 min at 30^0C. Phosphorylation was analyzed by autoradiography (top panel). A Coomassie stained gel of the reaction products is shown (bottom panel). Right, quantification of phosphorylation data (n=3). Data are expressed as mean ± SEM. $^{**}P < 0.01$ by paired Student's *t*-test. **(B)** Effect of increasing concentrations of ERK3 on the phosphorylation of SVIL. *In vitro* phosphorylation assays were performed as in A. **(C)** *In vitro* phosphorylation of MK5 by ERK3. His_6-MK5 was produced in *E. coli* and incubated with recombinant active ERK3 in the presence of radioactive ATP for 30 min at 30^0C. Phosphorylation was analyzed by autoradiography (top panel). Right, quantification of phosphorylation data (n=2). **(D)** *In vitro* phosphorylation assay of SVIL by different MAP kinases. Immunopurified SVIL was dephosphorylated with Lambda phosphatase prior to incubation with recombinant active ERK3,

ERK4 or ERK1 in the presence of radioactive ATP for 30 min at 30^0C (upper panels). A similar assay was runned in parallel using the common MAP kinase substrate MBP as control of MAP kinase activity (lower panels). Phosphorylation was analyzed by autoradiography. Right, quantification of phosphorylation data (n=3). Data are expressed as mean ± SEM. ***$P < 0.001$ by one-way ANOVA with Bonferroni post hoc test. **(E)** MS/MS spectrum showing the *in vitro* phosphorylation of SVIL on Ser245 by ERK3 (n=2). **(F)** Domain structure and amino acid alignment of the sequence surrounding Ser245 in mammalian SVIL isoforms. **(G)** *In vitro* phosphorylation assay. Immunopurified SVIL wild type or S245A was dephosphorylated with Lambda phosphatase (LPP) and incubated with recombinant active ERK3 for 30 min at 30^0C. The beads were then treated or not with LPP, and phosphorylation was analyzed by immunoblotting with phospho-SVIL(S245) antibody. Bottom, quantification of phosphorylation data (n=3). Data are expressed as mean ± SEM. ***$P < 0.001$ by one-way ANOVA with Bonferroni post hoc test. ns, non significant.

Figure 3. ERK3 interacts with and phosphorylates SVIL on S245 in intact cells

(A) Co-immunoprecipitation assay of ERK3 with SVIL. HEK 293T cells were co-transfected with the indicated ERK3 and SVIL constructs, and cell lysates were subjected to immunoprecipitation with anti-SVIL monoclonal antibody or IgG isotype control (CTL) antibody. Proteins were analyzed by immunoblotting (n=3). **(B)** Co-immunoprecipitation of endogenous ERK3 and SVIL. Hs578T cells were subjected to immunoprecipitation with anti-ERK3 monoclonal antibody or IgG isotype control antibody and analyzed by immunoblotting (n=3). **(C)** Co-immunoprecipitation assay of ERK3 domains with SVIL. HEK 293T cells were co-transfected with Flag-SVIL and either Myc_6-tagged ERK3 full-length, ERK3(1-365) (N-teminus) or ERK3(365-721) (C-terminus) constructs. SVIL was then immunoprecipitated with anti-Flag antibody and the proteins were analyzed by immunoblotting (n=3). **(D)** *In vivo*

phosphorylation assay. HEK 293T cells were co-transfected with Myc_6-ERK3 and Flag-SVIL wild type or S245A constructs. SVIL was immunoprecipitated with anti-Flag antibody and phosphorylation was analyzed by immunoblotting with anti-phospho-SVIL(S245) or anti-phospho-motif(PXSP) antibodies. Right, quantification of phosphorylation data (n=3). Data are expressed as mean ± SEM. *$P < 0.05$, **$P < 0.01$, ***$P < 0.001$ by one-way ANOVA with Bonferroni post hoc test. **(E)** Effect of ERK3 depletion on the i*n vivo* phosphorylation of SVIL. Hs578T cells were treated with non-target (NT) or *MAPK6* siRNAs for 24 h, and then transfected with Flag-SVIL. SVIL was immunoprecipitated with anti-Flag antibody and phosphorylation was analyzed by immunoblotting with anti-phospho-SVIL(S245) antibody. Right, quantification of phosphorylation data (n=3). Data are expressed as mean ± SEM. **$P <$ 0.01 by paired Student's *t*-test. ns, non significant.

Figure 4. ERK3 kinase activity controls the ploidy of breast cancer epithelial cells

(A) Hs578T cells were transfected with Flag-SVIL and treated with 5 μM ERK3 inhibitor for 24 h. SVIL was immunoprecipitated with anti-Flag antibody and phosphorylation was analyzed by immunoblotting with anti-phospho-SVIL(S245) antibody (n=2). **(B-C)** Hs578T cells were depleted of SVIL by CRISPR/Cas9 gene editing (see Fig. 5A). Control (CTL) or SVIL-depleted (SVIL KD) cell populations were treated with vehicle (DMSO) or the indicated concentrations of ERK3 inhibitor for 24 h. **(B)** The frequency of multinucleated cells was scored by fluorescence microscopy after phalloidin and Hoechst 33342 staining. A total of 1,508-1,942 cells were analyzed for each experimental condition. Results are expressed as mean ± SEM (n=3 biological replicates). *$P < 0.05$, **$P < 0.01$ by Student's t-test. ns, non significant. **(C)** Representative images of treated cells after phalloidin and Hoechst 33342 staining. Arrows indicate multinucleated cells. Scale bar = 10 μm.

Figure 5. ERK3 controls cell ploidy through phosphorylation of SVIL

Hs578T cells were depleted of ERK3 (MAPK6 KD) or SVIL (SVIL KD) by CRISPR/Cas9 gene editing. Control, ERK3- and SVIL-depleted cell pools were transfected with EGFP alone or EGFP-SVIL wild type, S245A or S245D. **(A)** Immunoblot analysis of Hs578T edited cells. **(B)** The frequency of EGFP-positive multinucleated cells was scored by fluorescence microscopy after EGFP, Hoechst 33342 and phalloidin staining. A total of 799 to 1,511 cells were analyzed for each experimental condition. Results are expressed as mean ± SEM (n=4 biological replicates). *$P < 0.05$, **$P < 0.01$ by two-way ANOVA with Dunnett's post hoc test. ns, non significant. **(C)** Representative images of treated cells after EGFP, Hoescht 33342 and phalloidin staining are shown. Arrows indicate multinucleated cells. Scale bar = 50 μm.

Figure 6. Phosphorylation of SVIL by ERK3 regulates cytokinesis

(A) Cytokinesis failure in control, ERK3- and SVIL-depleted Hs578Tcells transfected or not with EGFP-SVIL wild type, S245A or S245D was quantified by time-lapse imaging of dividing cells. A total of 25-65 cells were scored for each condition (n>3 biological replicates). *$P < 0.05$, **$P < 0.01$ by Fisher's exact test. **(B)** Representative stills of movies S1-3 of control, ERK3- or SVIL-depleted Hs578T cells expressing Citrine-α-Tubulin 1B and H2B-mRFP. Time from anaphase onset (in min) is shown at the top left of each still. Scale bar = 10 μm. **(C-D)** Representative stills of movies of SVIL-depleted (C) or ERK3-depleted (D) Hs578T cells expressing EGFP-SVIL wild type, S245A or S245D forms of SVIL, and H2B-mRFP. Time from anaphase onset (in min) is shown at the top. Scale bar = 10 μm. **(E)** The expression level of EGFP-SVIL wild type, S245A or S245D forms in transfected control, ERK3- or SVIL-depleted Hs578T cells was quantified by measuring total GFP fluorescence intensity (a.u.) in individual cells and plotted as a function of the cell's ability to complete (success) or not (failure) cytokinesis. Pair-wise comparison (two-way ANOVA with Bonferonni post hoc test)

between success or failure for the three different SVIL constructs is shown. ***$P < 0.001$. ns, non significant.

Figure 7. ERK3 co-localizes with and phosphorylates SVIL in mitosis

(A) Maximal intensity projections of 5 confocal slices of fixed SVIL-depleted Hs578T cells co-transfected or not (-) with Myc_6-ERK3 and Flag-SVIL and stained with antibodies against Myc and Flag (n=3 biological replicates). Arrows show sites of co-localization of the Myc and Flag signals. In the right panels, actin (phalloidin, red) and nuclei (Hoechst 33342, blue) stainings inform on the different stages of cytokinesis. Scale bar = 10 μm. **(B)** Maximal intensity projections of 5 confocal slices of fixed control, ERK3-depleted and SVIL-depleted Hs578T cells stained with antibodies against endogenous ERK3 (green) and SVIL (magenta) (n=2 biological replicates). Arrow shows site of co-localization of ERK3 and SVIL signals. Actin (phalloidin, red) and nuclei (Hoechst 33342, blue) stainings inform on the stage of cytokinesis. Scale bar = 10 μm. **(C)** Hs578T cells were synchronized in G1, S, G2 and M phase of the cell cycle. Cell lysates were prepared and analyzed by immunoblotting with the indicated antibodies. **(D)** Maximal intensity projection of 3 confocal slices of SVIL-depleted Hs578T cells complemented or not with EGFP-SVIL wild type or S245A mutant and stained with antibodies against phospho-SVIL(S245) (n=3 biological replicates). In the right panels, α-tubulin (white) and nuclei (Hoechst 33342, blue) stainings inform on the different stages of cytokinesis. Scale bar = 10 μm.

Figure 8. ERK3 regulates myosin II activation at the contractile ring

(A) Sum intensity projections of 3 confocal slices of dividing control Hs578T cells, ERK3-depleted or SVIL-depleted Hs578T cells stained for phospho-RLC(S19). Top panel, cells were transfected with EGFP alone. Middle and bottom panels, ERK3- or SVIL-depleted Hs578T

cells were complemented with EGFP-SVIL wild type, S245A or S245D forms. Nuclei are stained with Hoechst 33342 in the merged images. Scale bar = 10 μm. **(B)** Quantification of phospho-Ser19 RLC staining. A total of 7 to 14 cells were analyzed in each experiment (n=3 biological replicates). *$P < 0.05$, ***$P < 0.001$ by one-way ANOVA with Tukey's post hoc test. **(C)** The expression level of EGFP-SVIL S245A protein in transfected SVIL-depleted Hs578T cells was quantified by measuring GFP fluorescence intensity (a.u.) in individual cells and plotted as function of the measured phospho-Ser19 RLC ratio of the cell equator over the whole cell (n = 10). The coefficient of determination (R^2) is shown.

Table 1. Cellular component GO enrichment analysis of candidate ERK3 substrates

GO-term ID	GO-term description	Count in network	Strength	False discovery rate
GO:0015629	actin cytoskeleton	8 of 432	0.98	0.00035
GO:0005856	cytoskeleton	14 of 2068	0.54	0.0013
GO:0030496	midbody	5 of 165	1.19	0.0013
GO:0043232	intracellular non-membrane-bounded organelle	20 of 4005	0.41	0.0013
GO:0005622	intracellular	37 of 14286	0.13	0.0035
GO:0043229	intracellular oragnelle	34 of 12193	0.16	0.0058
GO:0005829	cytosol	20 of 4958	0.32	0.0078
GO:0005634	nucleus	24 of 6892	0.25	0.0090
GO:0005737	cytoplasm	32 of 11238	0.17	0.0090
GO:0010369	chromocenter	2 of 14	1.87	0.0090

SUPPLEMENTAL MATERIAL

SUPPLEMENTARY FIGURES

Figure S1. ERK3 regulates cell ploidy through phosphorylation of SVIL on Ser245

Figure S2. Loss of ERK3 does not affect the cellular ploidy of primary MEFs

Figure S3. CDK1 does not phosphorylate SVIL on Ser245 *in vitro*

Figure S4. Effect of ERK3 depletion on SVIL expression

SUPPLEMENTARY TABLES

Table S1. List of phosphorylation sites in Hs578T cells depleted or not of ERK3

Table S2. List of ERK3-regulated phosphosites in Hs578T cells

SUPPLEMENTARY MOVIES

Movie S1. Movie of control Hs578T cells expressing Citrine-α-Tubulin 1B (green) and H2B-mRFP (magenta). Images were captured at 8 min intervals and displayed at 4 frames per second.

Movie S2. Movie of ERK3-depleted Hs578T cells expressing Citrine-α-Tubulin 1B (green) and H2B-mRFP (magenta). Images were captured at 8 min intervals and displayed at 4 frames per second.

Movie S3. Movie of SVIL-depleted Hs578T cells expressing Citrine-α-Tubulin 1B (green) and H2B-mRFP (magenta). Images were captured at 8 min intervals and displayed at 4 frames per second.

Figure 1

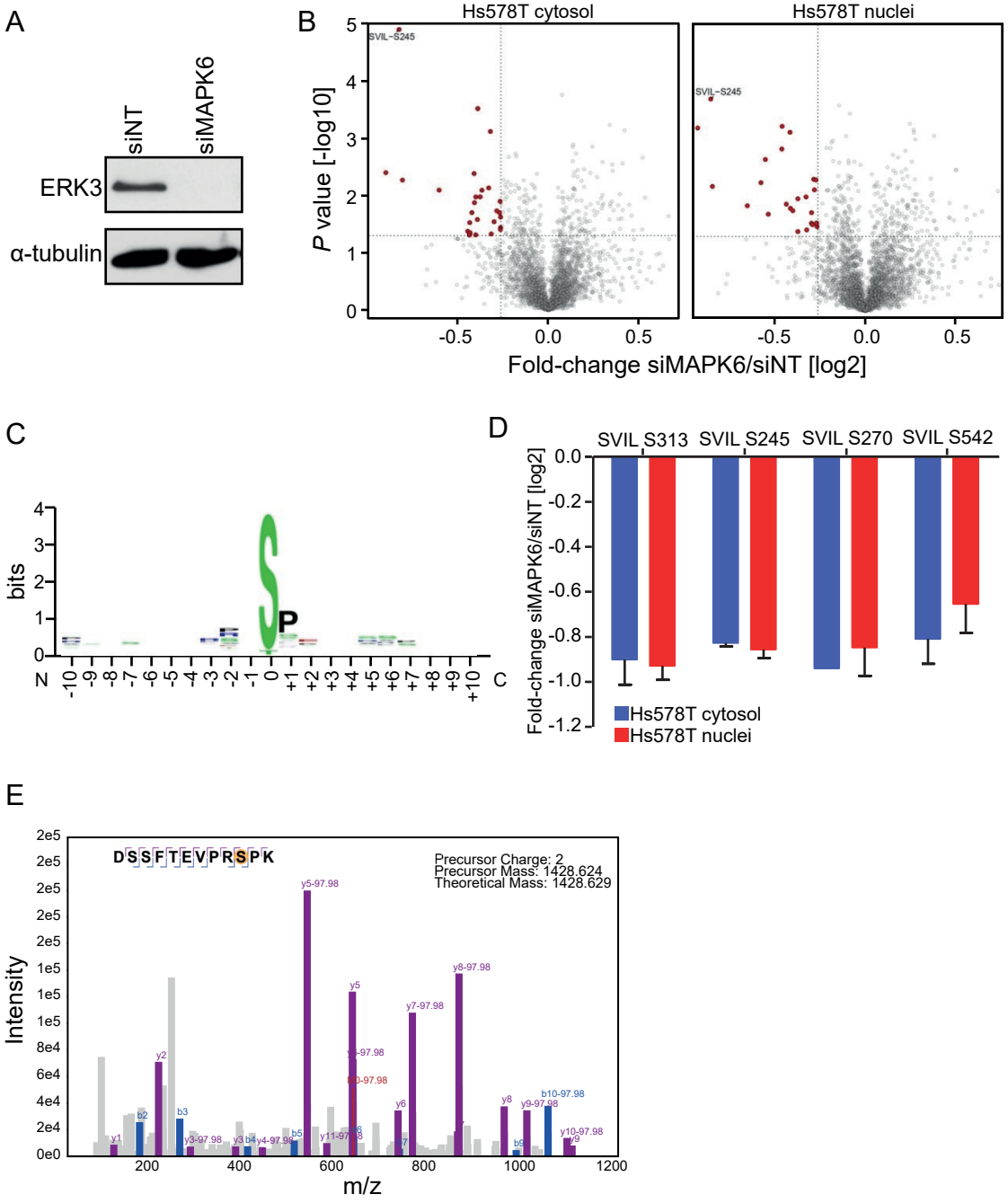

Figure 1. Quantitative phosphoproteomic profiling of ERK3 signaling network
(A) Representative immunoblot of ERK3 expression after RNAi-mediated depletion in Hs578T cells. (B) Volcano plot of quantitative changes in phosphopeptides in the cytosolic and nuclear fractions of ERK3-depleted Hs578T cells plotted as Log2 fold-change and P value. Phosphopeptides displaying a significant decrease in abundance (fold change ≥ 1.2 and $P < 0.05$, paired t-test) are highlighted in red. Data are from 4 biological replicates. (C) PhosphoLogo representation of ERK3-sensitive phosphosites. (D) SVIL phosphorylation sites showing significant changes (paired Student's t-test) upon depletion of ERK3 in Hs578T cells. Data are mean ± SEM (n=4). (E) MS/MS spectrum confirming the phosphorylation of SVIL on Ser245.

Figure 2

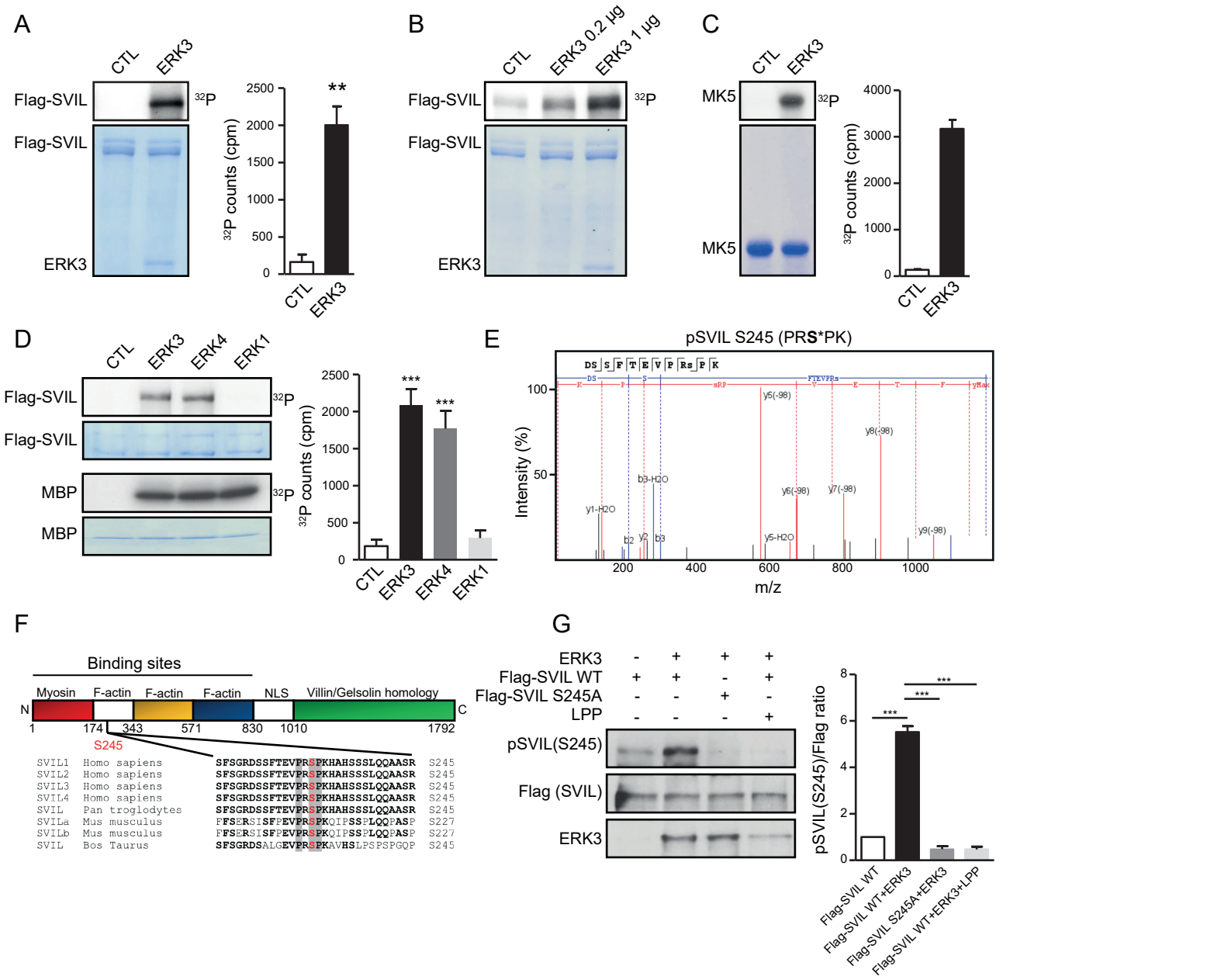

Figure 2. ERK3 directly phosphorylates SVIL on Ser245 in vitro
(A) In vitro phosphorylation assay. Immunopurified SVIL was dephosphorylated with Lambda phosphatase prior to incubation with recombinant active ERK3 in the presence of radioactive ATP for 30 min at 300C. Phosphorylation was analyzed by autoradiography (top panel). A Coomassie stained gel of the reaction products is shown (bottom panel). Right, quantification of phosphorylation data (n=3). Data are expressed as mean ± SEM. **P < 0.01 by paired Student's t-test. (B) Effect of increasing concentrations of ERK3 on the phosphorylation of SVIL. In vitro phosphorylation assays were performed as in A. (C) In vitro phosphorylation of MK5 by ERK3. His6-MK5 was produced in E. coli and incubated with recombinant active ERK3 in the presence of radioactive ATP for 30 min at 300C. Phosphorylation was analyzed by autoradiography (top panel). Right, quantification of phosphorylation data (n=2). (D) In vitro phosphorylation assay of SVIL by different MAP kinases. Immunopurified SVIL was dephosphorylated with Lambda phosphatase prior to incubation with recombinant active ERK3, ERK4 or ERK1 in the presence of radioactive ATP for 30 min at 300C (upper panels). A similar assay was runned in parallel using the common MAP kinase substrate MBP as control of MAP kinase activity (lower panels). Phosphorylation was analyzed by autoradiography. Right, quantification of phosphorylation data (n=3). Data are expressed as mean ± SEM. ***P < 0.001 by one-way ANOVA with Bonferroni post hoc test. (E) MS/MS spectrum showing the in vitro phosphorylation of SVIL on Ser245 by ERK3 (n=2). (F) Domain structure and amino acid alignment of the sequence surrounding Ser245 in mammalian SVIL isoforms. (G) In vitro phosphorylation assay. Immunopurified SVIL wild type or S245A was dephosphorylated with Lambda phosphatase (LPP) and incubated with recombinant active ERK3 for 30 min at 300C. The beads were then treated or not with LPP, and phosphorylation was analyzed by immunoblotting with phospho-SVIL(S245) antibody. Bottom, quantification of phosphorylation data (n=3). Data are expressed as mean ± SEM. ***P < 0.001 by one-way ANOVA with Bonferroni post hoc test. ns, non significant.

Figure 3

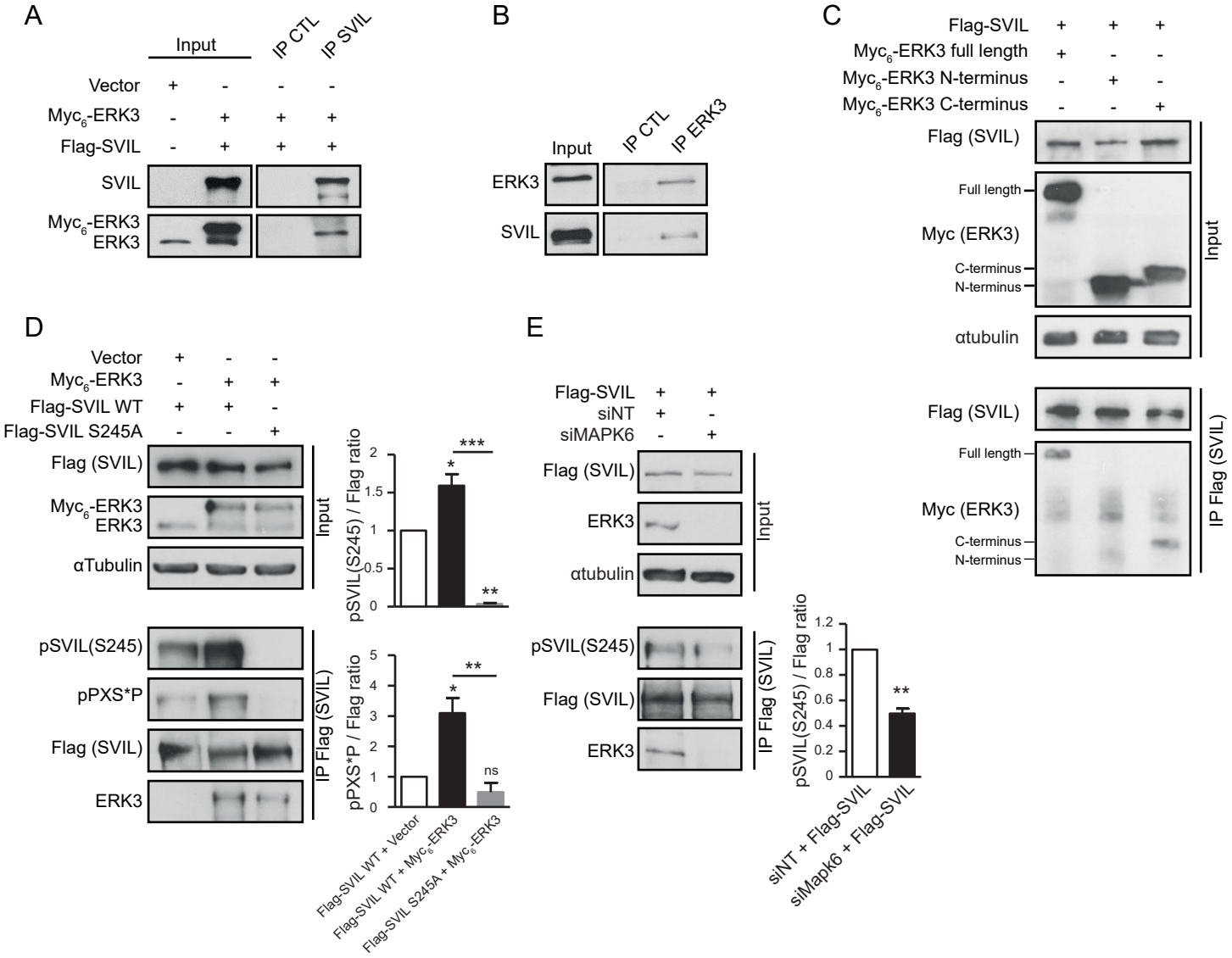

Figure 3. ERK3 interacts with and phosphorylates SVIL on S245 in intact cells
(A) Co-immunoprecipitation assay of ERK3 with SVIL. HEK 293T cells were co-transfected with the indicated ERK3 and SVIL constructs, and cell lysates were subjected to immunoprecipitation with anti-SVIL monoclonal antibody or IgG isotype control (CTL) antibody. Proteins were analyzed by immunoblotting (n=3). (B) Co-immunoprecipitation of endogenous ERK3 and SVIL. Hs578T cells were subjected to immunoprecipitation with anti-ERK3 monoclonal antibody or IgG isotype control antibody and analyzed by immunoblotting (n=3). (C) Co-immunoprecipitation assay of ERK3 domains with SVIL. HEK 293T cells were co-transfected with Flag-SVIL and either Myc6-tagged ERK3 full-length, ERK3(1-365) (N-teminus) or ERK3(365-721) (C-terminus) constructs. SVIL was then immunoprecipitated with anti-Flag antibody and the proteins were analyzed by immunoblotting (n=3). (D) In vivo phosphorylation assay. HEK 293T cells were co-transfected with Myc6-ERK3 and Flag-SVIL wild type or S245A constructs. SVIL was immunoprecipitated with anti-Flag antibody and phosphorylation was analyzed by immunoblotting with anti-phospho-SVIL(S245) or anti-phospho-motif(PXSP) antibodies. Right, quantification of phosphorylation data (n=3). Data are expressed as mean ± SEM. *P < 0.05, **P < 0.01, ***P < 0.001 by one-way ANOVA with Bonferroni post hoc test. (E) Effect of ERK3 depletion on the in vivo phosphorylation of SVIL. Hs578T cells were treated with non-target (NT) or MAPK6 siRNAs for 24 h, and then transfected with Flag-SVIL. SVIL was immunoprecipitated with anti-Flag antibody and phosphorylation was analyzed by immunoblotting with anti-phospho-SVIL(S245) antibody. Right, quantification of phosphorylation data (n=3). Data are expressed as mean ± SEM. **P < 0.01 by paired Student's t-test. ns, non significant.

Figure 4

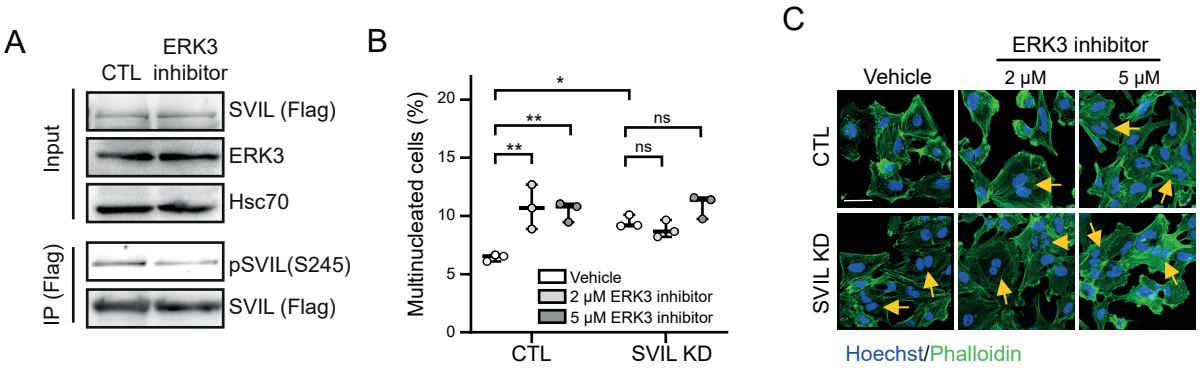

Figure 4. ERK3 kinase activity controls the ploidy of breast cancer epithelial cells
(A) Hs578T cells were transfected with Flag-SVIL and treated with 5 μM ERK3 inhibitor for 24 h. SVIL was immunoprecipitated with anti-Flag antibody and phosphorylation was analyzed by immunoblotting with anti-phospho-SVIL(S245) antibody (n=2). (B-C) Hs578T cells were depleted of SVIL by CRISPR/Cas9 gene editing (see Fig. 5A). Control (CTL) or SVIL-depleted (SVIL KD) cell populations were treated with vehicle (DMSO) or the indicated concentrations of ERK3 inhibitor for 24 h. (B) The frequency of multinucleated cells was scored by fluorescence microscopy after phalloidin and Hoechst 33342 staining. A total of 1,508-1,942 cells were analyzed for each experimental condition. Results are expressed as mean +/- SEM (n=3 biological replicates). *P < 0.05, **P < 0.01 by Student's t-test. ns, non significant. (C) Representative images of treated cells after phalloidin and Hoechst 33342 staining. Arrows indicate multinucleated cells. Scale bar = 10 μm.

Figure 5

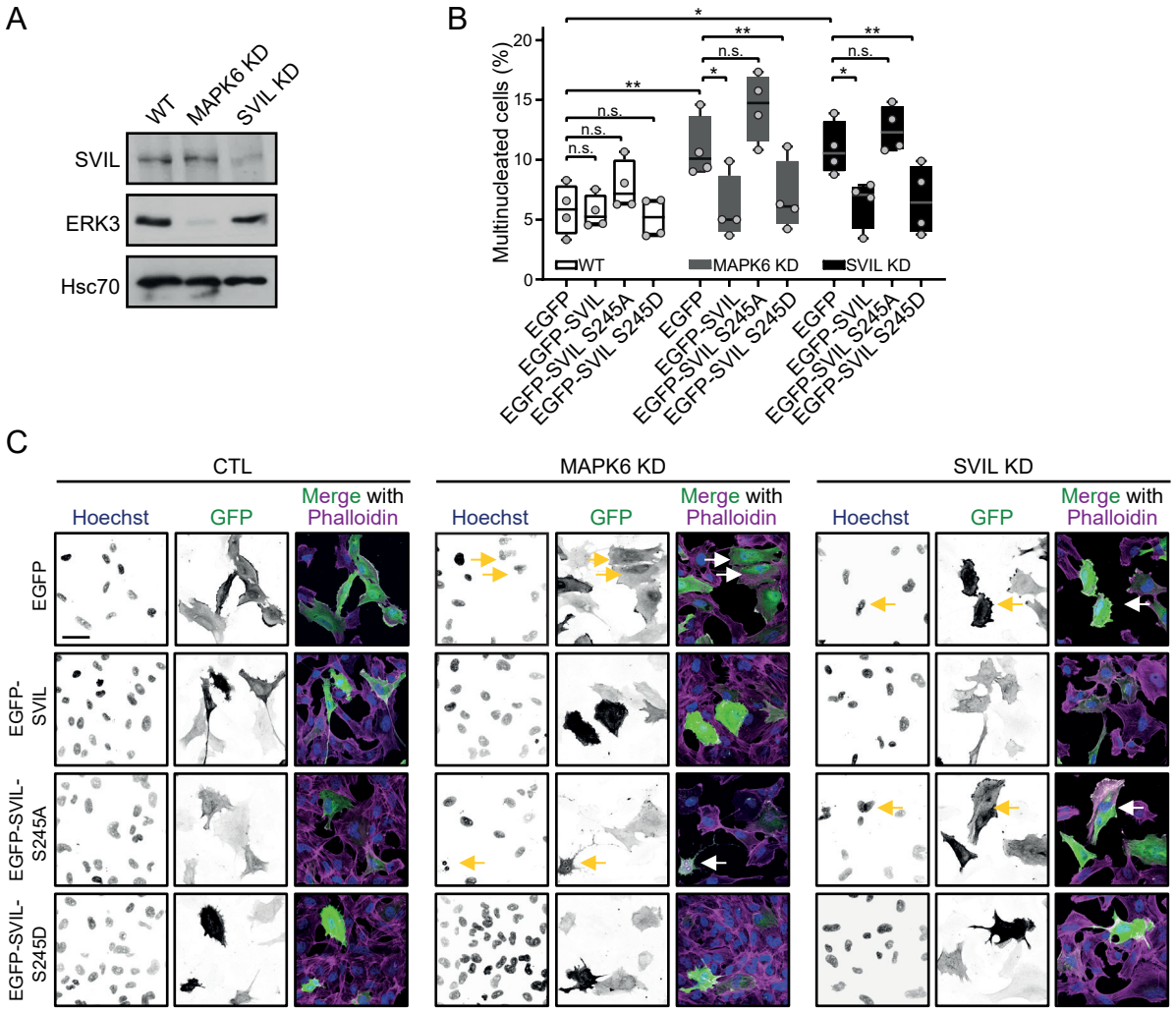

Figure 5. ERK3 controls cell ploidy through phosphorylation of SVIL
Hs578T cells were depleted of ERK3 (MAPK6 KD) or SVIL (SVIL KD) by CRISPR/Cas9 gene editing. Control, ERK3- and SVIL-depleted cell pools were transfected with EGFP alone or EGFP-SVIL wild type, S245A or S245D. (A) Immunoblot analysis of Hs578T edited cells. (B) The frequency of EGFP-positive multinucleated cells was scored by fluorescence microscopy after EGFP, Hoechst 33342 and phalloidin staining. A total of 799 to 1,511 cells were analyzed for each experimental condition. Results are expressed as mean +/- SEM (n=4 biological replicates). *P < 0.05, **P < 0.01 by two-way ANOVA with Dunnett's post hoc test. ns, non significant. (C) Representative images of treated cells after EGFP, Hoescht 33342 and phalloidin staining are shown. Arrows indicate multinucleated cells. Scale bar = 50 µm.

Figure 6

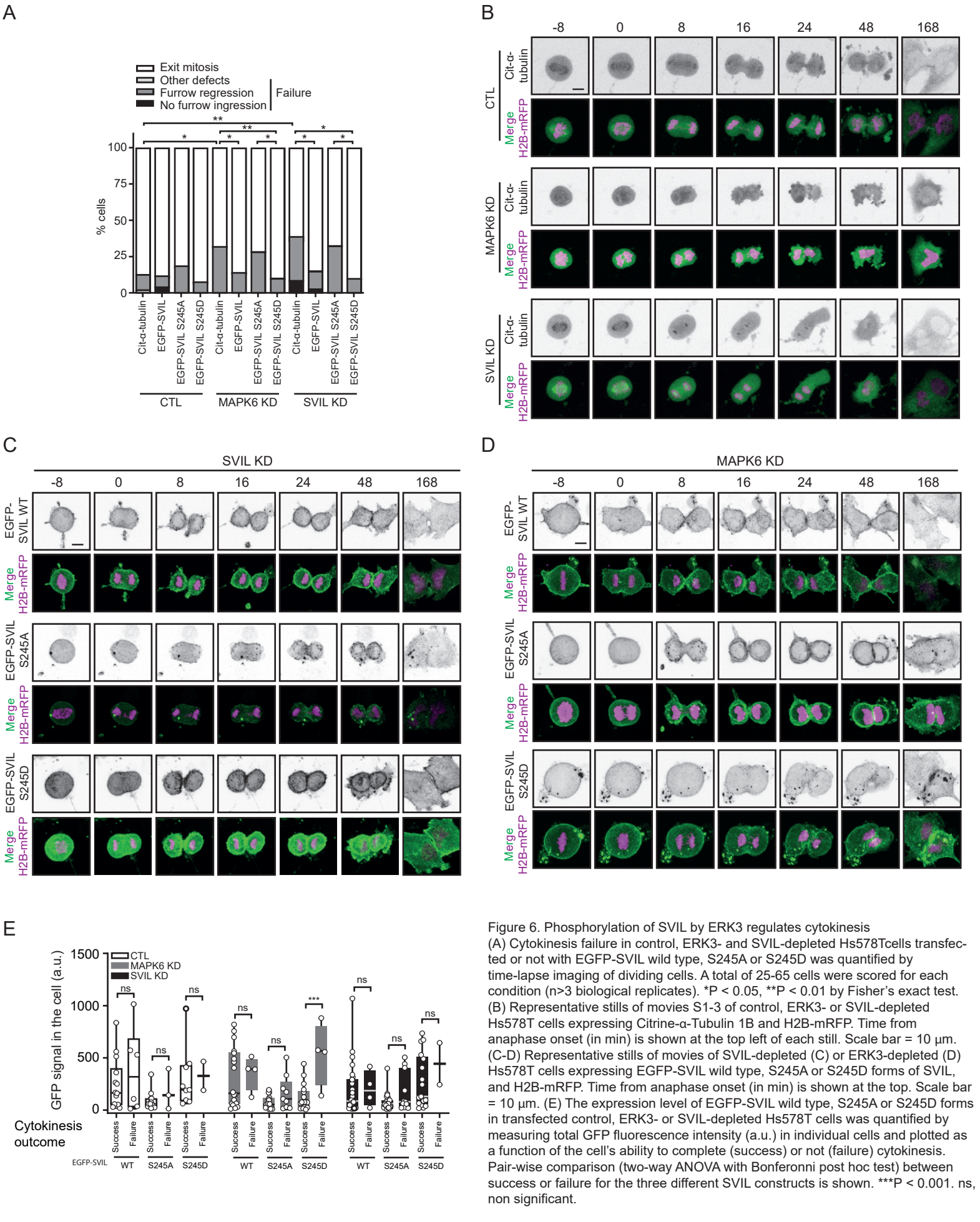

Figure 6. Phosphorylation of SVIL by ERK3 regulates cytokinesis
(A) Cytokinesis failure in control, ERK3- and SVIL-depleted Hs578Tcells transfected or not with EGFP-SVIL wild type, S245A or S245D was quantified by time-lapse imaging of dividing cells. A total of 25-65 cells were scored for each condition (n>3 biological replicates). *P < 0.05, **P < 0.01 by Fisher's exact test. (B) Representative stills of movies S1-3 of control, ERK3- or SVIL-depleted Hs578T cells expressing Citrine-α-Tubulin 1B and H2B-mRFP. Time from anaphase onset (in min) is shown at the top left of each still. Scale bar = 10 µm. (C-D) Representative stills of movies of SVIL-depleted (C) or ERK3-depleted (D) Hs578T cells expressing EGFP-SVIL wild type, S245A or S245D forms of SVIL, and H2B-mRFP. Time from anaphase onset (in min) is shown at the top. Scale bar = 10 µm. (E) The expression level of EGFP-SVIL wild type, S245A or S245D forms in transfected control, ERK3- or SVIL-depleted Hs578T cells was quantified by measuring total GFP fluorescence intensity (a.u.) in individual cells and plotted as a function of the cell's ability to complete (success) or not (failure) cytokinesis. Pair-wise comparison (two-way ANOVA with Bonferonni post hoc test) between success or failure for the three different SVIL constructs is shown. ***P < 0.001. ns, non significant.

Figure 7

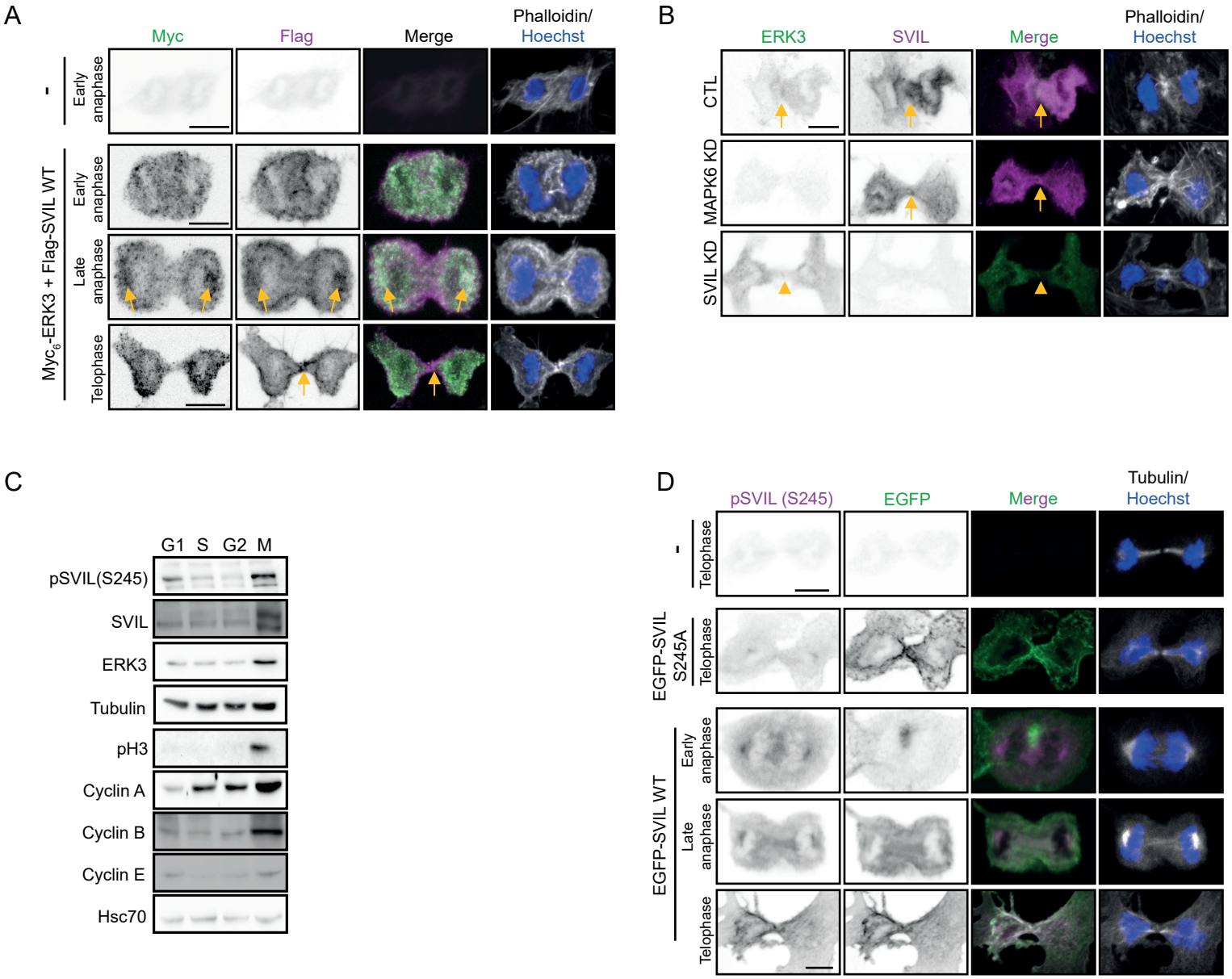

Figure 7. ERK3 co-localizes with and phosphorylates SVIL in mitosis
(A) Maximal intensity projections of 5 confocal slices of fixed SVIL-depleted Hs578T cells co-transfected or not (-) with Myc6-ERK3 and Flag-SVIL and stained with antibodies against Myc and Flag (n=3 biological replicates). Arrows show sites of co-localization of the Myc and Flag signals. In the right panels, actin (phalloidin, red) and nuclei (Hoechst 33342, blue) stainings inform on the different stages of cytokinesis. Scale bar = 10 µm. (B) Maximal intensity projections of 5 confocal slices of fixed control, ERK3-depleted and SVIL-depleted Hs578T cells stained with antibodies against endogenous ERK3 (green) and SVIL (magenta) (n=2 biological replicates). Arrow shows site of co-localization of ERK3 and SVIL signals. Actin (phalloidin, red) and nuclei (Hoechst 33342, blue) stainings inform on the stage of cytokinesis. Scale bar = 10 µm. (C) Hs578T cells were synchronized in G1, S, G2 and M phase of the cell cycle. Cell lysates were prepared and analyzed by immunoblotting with the indicated antibodies. (D) Maximal intensity projection of 3 confocal slices of SVIL-depleted Hs578T cells complemented or not with EGFP-SVIL wild type or S245A mutant and stained with antibodies against phospho-SVIL(S245) (n=3 biological replicates). In the right panels, α-tubulin (white) and nuclei (Hoechst 33342, blue) stainings inform on the different stages of cytokinesis. Scale bar = 10 µm.

Figure 8

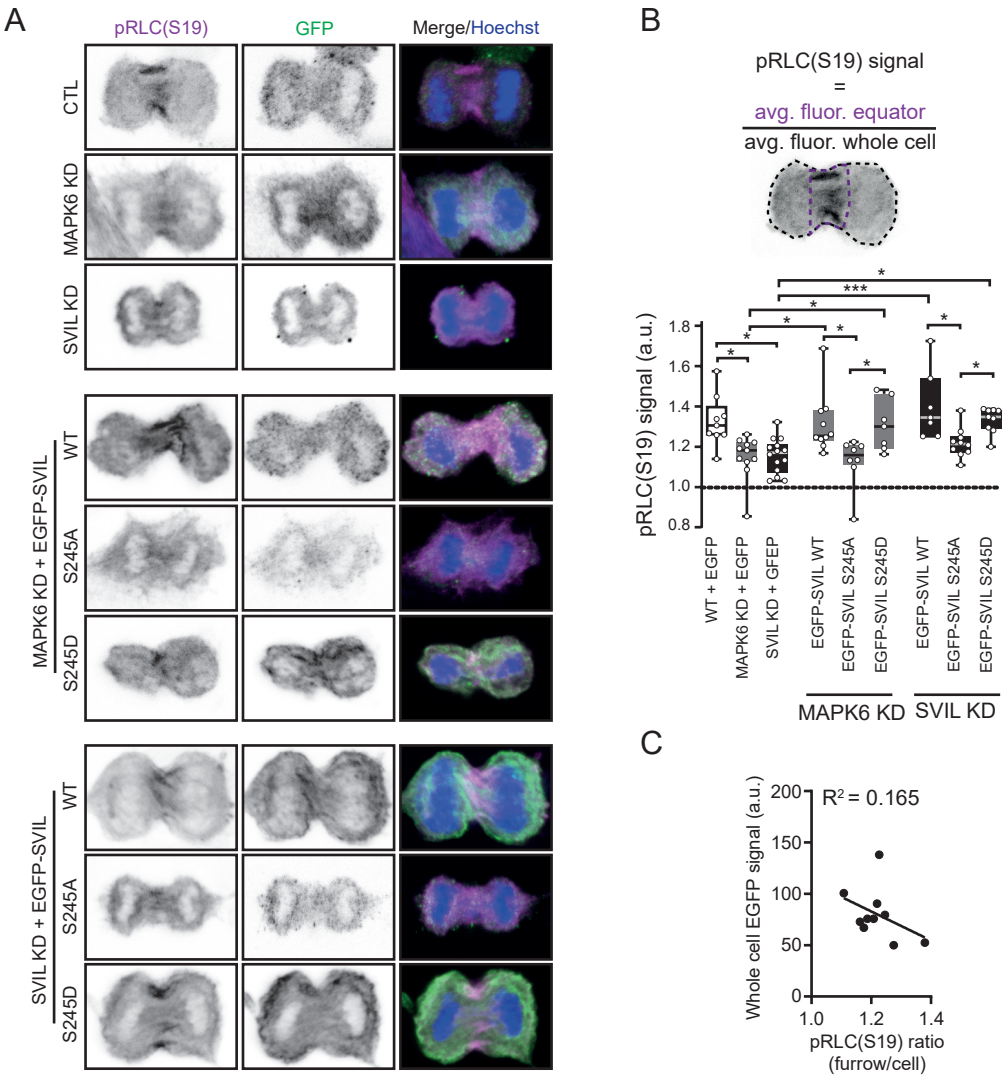

Figure 8. ERK3 regulates myosin II activation at the contractile ring
(A) Sum intensity projections of 3 confocal slices of dividing control Hs578T cells, ERK3-depleted or SVIL-depleted Hs578T cells stained for phospho-RLC(S19). Top panel, cells were transfected with EGFP alone. Middle and bottom panels, ERK3- or SVIL-depleted Hs578T cells were complemented with EGFP-SVIL wild type, S245A or S245D forms. Nuclei are stained with Hoechst 33342 in the merged images. Scale bar = 10 μm. (B) Quantification of phospho-Ser19 RLC staining. A total of 7 to 14 cells were analyzed in each experiment (n=3 biological replicates). *P < 0.05, ***P < 0.001 by one-way ANOVA with Tukey's post hoc test. (C) The expression level of EGFP-SVIL S245A protein in transfected SVIL-depleted Hs578T cells was quantified by measuring GFP fluorescence intensity (a.u.) in individual cells and plotted as function of the measured phospho-Ser19 RLC ratio of the cell equator over the whole cell (n = 10). The coefficient of determination (R2) is shown.